Uncertainty quantification of input matrices and transfer function in input/output subspace system identification

Szymon Gres, Michael Döhler, Niels-Jørgen Jacobsen, Laurent Mevel

HAL Id: hal-03607852
https://inria.hal.science/hal-03607852

Submitted on 14 Mar 2022

Uncertainty quantification of input matrices and transfer function in input/output subspace system identification☆

Szymon Greś[a,*], Michael Döhler[a], Niels-Jørgen Jacobsen[b], Laurent Mevel[a]

[a]*Univ. Gustave Eiffel, Inria, COSYS/SII, I4S, Campus de Beaulieu, 35042 Rennes, France*
[b]*Hottinger Brüel & Kjær A/S, DK-2850 Nærum, Denmark*

Abstract

The transfer function of a linear mechanical system can be defined in terms of the quadruplet of state-space matrices (A, B, C, D) that can be identified from input and output measurements with subspace-based system identification methods. The estimation of the quadruplet has been well studied in the literature from both theoretical and practical viewpoints. Nonetheless, a practical algorithm for uncertainty quantification of its estimation errors and the uncertainty of the resultant parametric transfer function is missing in the context of subspace identification. For several output-only and input/output subspace methods, the covariance related to the matrices (A, C) and to the resulting modal parameters can be effectively obtained with recently developed first-order perturbation-based schemes, while the corresponding uncertainty quantification for the input-related matrices (B, D) is missing. In this paper, explicit expressions for the covariance related to matrices (B, D) are developed, and applied to the covariance estimation of the resulting transfer function. The proposed schemes are validated on simulated data of a mechanical system and are applied to laboratory measurements of a plate.

Keywords: Linear time-invariant systems, subspace methods, input/output data, transfer function, variance computation

1. Introduction

The identification of dynamic system characteristics from vibration measurements is a fundamental task in engineering. Amongst others, subspace-based system identification methods are well-suited for this purpose, identifying the system matrices of a linear time-invariant state-space model that describes the dynamic system behavior [2]. Besides the unknown ambient excitation forces acting on a structure, some of the input forces are available in different engineering applications, such as shaker tests of bridges [3], structural health monitoring of wind turbine blades [4–6], aircraft control [7, 8] and various laboratory

---

testing applications. Then, input/output system identification methods – also called combined deterministic-stochastic identification methods – identify the complete set of system matrices (A, B, C, D) of the structural system from data [2, 9], where the knowledge of inputs enhances the identification performance [10]. These matrices can be used to evaluate the transfer function of the system, which is oftentimes required in methods e.g. for damage detection [11, 12], damage localization [13, 14] model updating [15, 16], and modal scaling [9, 17].

The practical value of identifying parameters from data is significantly increased if the deployed identification procedure provides their confidence bounds. The information about their (co-)variance is only useful when the underlying identification algorithm is consistent, that is when the estimated parameters converge to their true values as the amount of data tends to infinity. This is the case for the family of subspace methods, which are consistent when the noise driving the system is stationary [18, 19] or non-stationary [20]. Furthermore, their asymptotic normality has been shown and theoretical expressions for their asymptotic covariances were derived e.g. in [21–24]. Use of those expressions for the actual covariance estimation is problematic in practical applications, since they require in addition e.g. the estimation of the unknown states and their covariances, which are not necessary to estimate the quadruplet of state-space matrices (A, B, C, D) nor the modal parameters of the underlying mechanical system. A different approach was proposed in [25, 26], where the covariance of estimated parameters is computed easily from the sample covariances of the underlying data correlations and related sensitivities, based on the first-order delta method. In the context of subspace identification of mechanical systems, explicit expressions for the covariances related to the state transition and observation matrices (A, C) and the corresponding modal parameter estimates have been proposed for output-only [10, 26–28] and for input/output methods [9, 10]. Case studies confirming the Gaussian characteristics of modal parameter estimates can be found e.g. in [29]. An algorithm for the covariance related to the estimates of (B, D) has been developed for the impulse response-based estimation and realization method (IREAR) in [30], under the assumption of fully known inputs and no unknown ambient excitation. More general systems that include noise inputs in addition to the known inputs can be identified using combined deterministic-stochastic input/output subspace methods, for which an explicit algorithm to obtain the covariance related to the estimates of (B, D) has not yet been derived. Moreover, the development of such an algorithm is a necessary step for uncertainty quantification of the transfer function estimated subsequently from the (A, B, C, D) quadruplet.

The uncertainty quantification and derivation of confidence bounds for transfer function estimates were given considerable attention in the past. For example, the asymptotic uncertainty of the rational transfer function was evaluated by means of the frequency domain Gaussian maximum likelihood estimator in [31, 32]. This estimator yields the lowest possible uncertainty for the transfer function estimation, however, unlike the subspace methods considered herein, it is not direct. A periodogram averaging approach was used to derive an asymptotic error bound of the empirical transfer function in [33]. The quality of the error

2

bounds estimated with this approach, however, relies heavily on the number of averages used to compute the confidence bounds of the transfer function estimates. Moreover, it assumes that the input is periodic, which is not always the case in practice. The mechanical transfer function evaluated along the complex frequency plane relates to the frequency response functions (FRFs), whose covariance computation was also considered in the past, for example by using coherence functions [34, 35], which is applied in the context of frequency domain modal parameter estimation [36]. However, the use of coherence functions to evaluate the covariance of FRFs requires that the noise on the estimated FRFs is circular-complex normally distributed and is uncorrelated over the frequencies [37], which is restrictive in practical applications. Moreover, the use of coherence functions for uncertainty quantification of FRFs can be problematic in presence of leakage errors and requires appropriate windowing techniques [38], and an additional modeling of the noise terms [39]. The first-order delta method was used for the uncertainty quantification of FRFs in [30], which involves no windowing nor averaging, thus is free of the aforementioned shortcomings. Therein, the FRFs are computed from estimates of the state-space system matrices (A, B, C, D) that are obtained with the IREAR method for systems without noise inputs [30]. As the covariance related to the system matrices depends on the used identification algorithm, this also the case for the resulting FRFs, for which two input/output subspace methods will be considered in this paper.

This paper contributes to uncertainty quantification of parameter estimates in system identification of mechanical systems with a perspicuous development of an explicit algorithm to obtain the covariances related to estimates of the input and feedthrough matrices (B, D) in input/output subspace system identification, and its application to the covariance computation of the parametric transfer function, including its magnitude and phase. The developments are shown based on two input/output algorithms, namely the data-driven N4SID algorithm [40] and the covariance-driven algorithm from [20], and can be easily extended to other input/output subspace methods. Like this, the theoretical results on consistency [20] and asymptotic normality [41] of the considered input/output subspace methods are complemented with a practical algorithm that allows the direct estimation of the related covariances. With the obtained covariance expressions, a practical tool is provided for uncertainty quantification in diverse applications related to e.g. damage detection and localization, model updating or modal scaling for methods that are based on the identification of input/output state-space matrices or the transfer function.

The paper is structured as follows. The system modeling is recalled in Section 2, and the identification of the system matrices (A, B, C, D) is presented in Section 3. In Section 4, the covariance expression for the estimates of (B, D) is derived, and the resultant covariance estimates are used to obtain the covariance of the transfer function. Both schemes are validated on a numerical example of a mechanical system in Section 5. Finally, the proposed uncertainty quantification framework is applied to compute the confidence intervals of a transfer function evaluated from laboratory measurements of a plate in Section 6. For easier reading, technical details of the derivations are kept in the Appendix.

3

2. System modeling

The dynamic behavior of a linear time-invariant system can be represented by a discrete-time state-space model of order n

$$x_{k+1} = Ax_k + Bu_k + w_k \; , \tag{1}$$

$$y_k = Cx_k + Du_k + v_k \; , \tag{2}$$

where $x_k \in \mathbb{R}^n$ are the states, $u_k \in \mathbb{R}^u$ are the known inputs, $A \in \mathbb{R}^{n \times n}$, $B \in \mathbb{R}^{n \times u}$, $C \in \mathbb{R}^{r \times n}$ and $D \in \mathbb{R}^{r \times u}$ are the state transition, output and feedthrough matrices. The input sequence $\{u_k\}$ is a quasi-stationary process. The sequences $\{w_k\}$ and $\{v_k\}$ are the process and output noises, respectively, possibly correlated to each other. They are assumed to be independent and identically distributed with zero mean, to have finite fourth moments and to be independent of the input. It is assumed that the noises and the input process are persistently exciting [42], and that there is no feedback from y_k to u_k. The system is assumed to be stable, observable and controllable, and eigenvalues of the state matrix A are assumed to be distinct. Some of the aforementioned assumptions are discussed in detail in [20].

Matrices (A, C) are of particular interest in modal analysis, since they are used to identify the eigenstructure of the underlying mechanical system and consequently its modal parameters, i.e. natural frequencies, damping ratios and mode shapes. Furthermore, matrices B and D are required to define the discrete transfer function $H(z)$ that is derived from a z-transform of (1)-(2), and it models the complete input-output dynamic behaviour of the system

$$H(z) = C(zI_n - A)^{-1}B + D \in \mathbb{C}^{r \times u}, \tag{3}$$

where I_n is the identity matrix of size $n \times n$. Evaluated at $z = e^{i\omega T_s}$, $0 \leq \omega \leq \omega_f$, where ω_f is the Nyquist frequency and T_s the discrete time step, $H(z)$ relates to the parametric discrete frequency response function. The quadruplet (A, B, C, D) can be identified with subspace methods based on geometric properties of input/output data. This requires expressing (1)-(2) in matrix input-output format, which alongside some notation is recalled next.

Definition 1 (Data matrix). *Let $a_k \in \mathbb{R}^b$ be a discrete signal at time step k. The parameter p defines the 'past' and 'future' data horizons. For $0 \leq i \leq j \leq 2p-1$ the data matrix $\mathcal{A}_{i|j}$ writes*

$$\mathcal{A}_{i|j} = \frac{1}{\sqrt{N}} \begin{bmatrix} a_i & a_{i+1} & \dots & a_{i+N-1} \\ a_{i+1} & a_{i+2} & \dots & a_{i+N} \\ \vdots & \vdots & \vdots & \vdots \\ a_j & a_{j+1} & \dots & a_{j+N-1} \end{bmatrix} \in \mathbb{R}^{(j-i+1)b \times N}. \tag{4}$$

4

From the input and output data, define the data matrices $\mathcal{Y}^- \in \mathbb{R}^{pr \times N}$, $\mathcal{Y}^+ \in \mathbb{R}^{pr \times N}$, $\mathcal{U}^- \in \mathbb{R}^{pu \times N}$, $\mathcal{U}^+ \in \mathbb{R}^{pu \times N}$ and $\mathcal{W}^- \in \mathbb{R}^{p(u+r) \times N}$

$$\mathcal{Y}^- = \mathcal{Y}_{0|p-1}, \ \mathcal{Y}^+ = \mathcal{Y}_{p|2p-1}, \ \mathcal{U}^- = \mathcal{U}_{0|p-1}, \ \mathcal{U}^+ = \mathcal{U}_{p|2p-1}, \ \mathcal{W}^- = \begin{bmatrix} \mathcal{U}^{-T} & \mathcal{Y}^{-T} \end{bmatrix}^T . \tag{5}$$

Furthermore, denote respectively the future and past block-row matrices for the system states as $\mathcal{X}^- = \mathcal{X}_{0|0}$, $\mathcal{X}^+ = \mathcal{X}_{p|p}$, and future and past output noise matrices as $\mathcal{V}^- = \mathcal{V}_{0|p-1}$, $\mathcal{V}^+ = \mathcal{V}_{p|2p-1}$. Data matrices $\mathcal{Y}^-$ and $\mathcal{Y}^+$ can be expressed by recursion of (1)-(2) as [2]

$$\mathcal{Y}^- = \Gamma \mathcal{X}^- + \overline{H}\mathcal{U}^- + \mathcal{V}^- , \tag{6}$$

$$\mathcal{Y}^+ = \Gamma \mathcal{X}^+ + \overline{H}\mathcal{U}^+ + \mathcal{V}^+ , \tag{7}$$

where $\Gamma \in \mathbb{R}^{pr \times n}$ and $\overline{H} \in \mathbb{R}^{pr \times pu}$ are respectively the extended observability matrix and lower block triangular Toeplitz matrix

$$\Gamma = \begin{bmatrix} C \\ CA \\ CA^2 \\ \vdots \\ CA^{p-1} \end{bmatrix}, \quad \overline{H} = \begin{bmatrix} D & 0 & 0 & \dots & 0 \\ CB & D & 0 & \dots & 0 \\ CAB & CB & D & \dots & 0 \\ \dots & \dots & \dots & \dots & \dots \\ CA^{p-2}B & CA^{p-3}B & CA^{p-4}B & \dots & D \end{bmatrix}, \tag{8}$$

which are used to identify (A, B, C, D) with an adequate projection of the measured data matrices, as shown in the following section. For their identification it is supposed that p is chosen such that the observability matrix without the last block row $\underline{\Gamma} \in \mathbb{R}^{(p-1)r \times n}$ is of full column rank, i.e. with at least $(p-1)r \geq n$.[1]

3. System identification

In subspace identification, the system matrices are obtained from a matrix $\mathcal{H}$ that is a consequence of a geometric projection of the data matrices (5) and depends on the chosen identification algorithm, see e.g. [2]. Therein, two general classes of identification algorithms exist, namely so-called *data-driven* and *covariance-driven* algorithms, which differ in the type of projection used to compute $\mathcal{H}$. In this section, the subspace-based identification of the system matrices is described, based on two different subspace methods as examples. The choice of the subspace method, i.e. the choice of $\mathcal{H}$, impacts the statistical properties of the estimates of (A, B, C, D), whose uncertainties are developed in the subsequent section.

---

[1]Note that $(p-1)r \geq n$ is a necessary condition for full column rank of $\underline{\Gamma}$. The theoretical sufficient condition is $p > n$.

3.1. Estimation of (A, C)

The estimation of (A, C) enclosed in this section is well-known, and recalled here for the sake of completeness. In the data-driven N4SID algorithm [40], $\mathcal{H}$ is defined by an oblique projection of the data matrices $\mathcal{Y}^+$ onto $\mathcal{W}^-$ along $\mathcal{U}^+$ as

$$\mathcal{H}_{\text{dat}} = \mathcal{Y}^+ /_{\mathcal{U}^+} \mathcal{W}^- = (\mathcal{Y}^+/\mathcal{U}^{+\perp})(\mathcal{W}^-/\mathcal{U}^{+\perp})^\dagger \mathcal{W}^- \ , \tag{9}$$

where the data matrices are defined in (5), $(\cdot)^\dagger$ denotes the pseudoinverse, and the orthogonal projection of a data matrix $\mathcal{A}$ onto the orthogonal complement of $\mathcal{B}$ is defined by $\mathcal{A}/\mathcal{B}^\perp = \mathcal{A} - \mathcal{A}/\mathcal{B} = \mathcal{A} - \mathcal{A}\mathcal{B}^T(\mathcal{B}\mathcal{B}^T)^{-1}\mathcal{B}$.

Several covariance-driven candidates for $\mathcal{H}$ were proposed in the past [10, 43, 44]. Herein, $\mathcal{H}$ for the covariance-driven case is defined with the orthogonal projection of data matrices after [44] as

$$\mathcal{H}_{\text{cov}} = \left(\mathcal{Y}^+/\mathcal{U}^{+\perp}\right) \mathcal{Y}^{-T} \ . \tag{10}$$

For both considered methods, an estimate of Γ can be retrieved from $\mathcal{H}$ by a Singular Value Decomposition truncated at model order n,

$$\mathcal{H} = \begin{bmatrix} \widehat{U}_{\text{s}} & \widehat{U}_{\text{ker}} \end{bmatrix} \begin{bmatrix} \widehat{D}_{\text{s}} & 0 \\ 0 & \widehat{D}_{\text{ker}} \end{bmatrix} \widehat{V}^T, \ \widehat{\Gamma} = \widehat{U}_{\text{s}}\widehat{D}_{\text{s}}^{1/2}. \tag{11}$$

An estimate of the observation matrix C is then obtained from the first block-row of $\widehat{\Gamma}$. The state transition matrix A is estimated from the shift invariance property of $\widehat{\Gamma}$, namely $\widehat{A} = \widehat{\underline{\Gamma}}^\dagger \widehat{\overline{\Gamma}}$, where $\widehat{\overline{\Gamma}}, \widehat{\underline{\Gamma}} \in \mathbb{R}^{(p-1)r \times n}$ are respectively the matrix $\widehat{\Gamma}$ without the first and the last block rows.

Remark 2. *The consistency of the estimates of (A, C) has been proven for both considered algorithms in [20] under the current assumptions. Note that any other subspace method described in [20] could be similarly envisioned, leading also to consistent estimates. The consistency holds up to a change of the state-space basis, which is set when obtaining $\widehat{\Gamma}$ through the SVD of $\mathcal{H}$. It is always possible to transform the estimates of (A, C) to a canonical form, e.g. into the modal basis [45] using a fixed mode shape scaling [46, 47]. Subsequently, the covariance related to estimates of (A, C) is obtained with respect to the same basis as the estimates of (A, C) in Section 4.2 when computing the transfer function covariance. The estimates of (B, D) and their related covariance are also obtained in the same basis in the next sections.*

3.2. Estimation of (B, D)

The estimation of the input matrix B and feedthrough matrix D was sketched in [48], amongst other algorithms discussed later, and is developed in detail in this section. Furthermore, their consistency is shown.

Matrices B and D can be obtained based on the input/output data relation (7) using the fact that the future sensor noise term is uncorrelated with the known future inputs, namely $\mathrm{E}[\mathcal{V}^+(\mathcal{U}^+)^T] = 0$. Define the data covariance matrices

$$\widehat{\mathcal{R}}_1 = \mathcal{Y}^+\mathcal{U}^{+T} \in \mathbb{R}^{pr \times pu}, \quad \widehat{\mathcal{R}}_2 = \mathcal{U}^+\mathcal{U}^{+T} \in \mathbb{R}^{pu \times pu}, \tag{12}$$

and recall the general input/output data matrix equation $\mathcal{Y}^+ = \Gamma\mathcal{X}^+ + \overline{H}\mathcal{U}^+ + \mathcal{V}^+$ from (7). Multiplying it with $\widehat{U}_{\ker}^T$ (see (11)) from the left and with $\mathcal{U}^{+T}$ from the right yields

$$\widehat{U}_{\ker}^T\widehat{\mathcal{R}}_1 = \underbrace{\widehat{U}_{\ker}^T\Gamma}_{\to 0} \mathcal{X}^+\mathcal{U}^{+T} + \widehat{U}_{\ker}^T\overline{H}\widehat{\mathcal{R}}_2 + \widehat{U}_{\ker}^T\underbrace{\mathcal{V}^+\mathcal{U}^{+T}}_{\to 0}, \tag{13}$$

$$\widehat{U}_{\ker}^T\widehat{\mathcal{R}}_1\widehat{\mathcal{R}}_2^{-1} = \widehat{U}_{\ker}^T\overline{H} + o(1) \tag{14}$$

where $o(1)$ is a matrix whose norm converges to zero if $N \to \infty$. Note that $\mathcal{R}_2$ is invertible since the input is assumed to be a persistently exciting quasi-stationary stochastic process. Denote the left hand side of (14) as $\widehat{\mathcal{M}} \in \mathbb{R}^{(pr-n) \times pu}$ and partition it to p block columns as

$$\widehat{\mathcal{M}} = \widehat{U}_{\ker}^T\widehat{\mathcal{R}}_1\widehat{\mathcal{R}}_2^{-1} = \left[\widehat{\mathcal{M}}_1 \ \ldots \ \widehat{\mathcal{M}}_p\right], \ \widehat{\mathcal{M}}_k \in \mathbb{R}^{(pr-n) \times u}, \ k = 1 \ldots p \ . \tag{15}$$

Similarly partition $\widehat{U}_{\ker}^T = \left[\widehat{\mathcal{L}}_1 \ \ldots \ \widehat{\mathcal{L}}_p\right]$, $\widehat{\mathcal{L}}_k \in \mathbb{R}^{(pr-n) \times r}$. Rearranging (14) and plugging in (8) leads then to the factorization

$$\underbrace{\begin{bmatrix} \widehat{\mathcal{M}}_1 \\ \widehat{\mathcal{M}}_2 \\ \widehat{\mathcal{M}}_3 \\ \vdots \\ \widehat{\mathcal{M}}_p \end{bmatrix}}_{=\widehat{\mathcal{M}}^v} = \underbrace{\begin{bmatrix} \widehat{\mathcal{L}}_1 & \widehat{\mathcal{L}}_2 & \ldots & \widehat{\mathcal{L}}_{p-1} & \widehat{\mathcal{L}}_p \\ \widehat{\mathcal{L}}_2 & \widehat{\mathcal{L}}_3 & \ldots & \widehat{\mathcal{L}}_p & 0 \\ \widehat{\mathcal{L}}_3 & \widehat{\mathcal{L}}_4 & \ldots & 0 & 0 \\ \ldots & \ldots & \ldots & \ldots & \ldots \\ \widehat{\mathcal{L}}_p & 0 & \ldots & 0 & 0 \end{bmatrix}}_{=\widehat{L}} \underbrace{\begin{bmatrix} I_r & 0 \\ 0 & \Gamma \end{bmatrix}}_{=O_s} \begin{bmatrix} D \\ B \end{bmatrix} + o(1), \tag{16}$$

where $\widehat{\mathcal{M}}^v \in \mathbb{R}^{p(pr-n) \times u}$, $\widehat{L} \in \mathbb{R}^{p(pr-n) \times pr}$ and $\widehat{O}_s \in \mathbb{R}^{pr \times (r+n)}$. Estimates of the matrices (B, D) follow as the least-squares solution

$$\begin{bmatrix} \widehat{D} \\ \widehat{B} \end{bmatrix} = \widehat{L}_s^\dagger \, \widehat{\mathcal{M}}^v, \tag{17}$$

where $\widehat{L}_s = \widehat{L}\widehat{O}_s$, and $\widehat{O}_s$ is obtained by plugging in the estimate $\widehat{\Gamma}$.

Remark 3. *The consistency of the estimates of (B, D) from (17) follows from the consistency of $\widehat{\mathcal{R}}_1$, $\widehat{\mathcal{R}}_2$ and $\widehat{\Gamma}$ [20] under the made assumptions. Matrix $\widehat{U}_{\ker}$ is derived from $\widehat{\Gamma}$ by the SVD and therefore a consistent left null space estimate (following from [49]), leading to consistency of $\widehat{\mathcal{M}}^v$ and $\widehat{L}$. In Appendix A it is proven that L has full column rank, hence $L_s = LO_s$ has full column rank due to full column rank of $\underline{\Gamma}$, and*

the consistency of $\widehat{B}$ and $\widehat{D}$ in (17) follows (up to a basis change). Note that while the feedthrough matrix D is independent of the state-space basis, the input matrix B is estimated in the same basis as (A, C) due to (16). Hence, the choice of a particular basis could be enforced following Remark 2. Subsequently, the related covariances are obtained with respect to the same basis as the underlying estimates in the next section.

Remark 4. *There are parallels between the applied approach and the algorithm to estimate B and D proposed in [43]. The approach in [43] uses the property $\mathrm{E}[\mathcal{V}^+\mathcal{Y}^{-T}] = 0$ to cancel the noise term in (7), and therefore multiplies (7) with $\mathcal{Y}^{-T}$ instead of $\mathcal{U}^{+T}$. However, when $\mathcal{U}^+$ is a white noise process as often assumed in theory, then the term $\mathcal{U}^+\mathcal{Y}^{-T}$ in the resulting product converges to zero, and consequently the estimation of (B, D) becomes impossible. Moreover, when $u > r$ the product $\mathcal{U}^+\mathcal{Y}^{-T}$ is not full row rank, so the operation analogous to (14) becomes invalid. The approach described above is free of those shortcomings.*

Furthermore, several schemes to estimate (B, D) were proposed in [2]. Compared to the methods therein, the approach described above does not involve computing the Kalman gain and estimating the state sequences, nor pseudoinverting large Kronecker products, which is appealing from the practical viewpoint. Most importantly, the expression used herein to estimate (B, D) is direct and simple, which allows to apply the first-order delta method to characterize their statistical distribution properties. These properties are a function of $\mathcal{H}_{\mathrm{cov}}$ or $\mathcal{H}_{\mathrm{dat}}$, which is investigated in the next section.

4. Covariance propagation to (B, D) and $H(z)$

Covariance estimates related to (B, D) and $H(z)$ are obtained based on the first-order delta method [50]. This statistical framework allows to characterize the probability distribution of a function of an asymptotically Gaussian variable based on one data set in order to obtain covariance estimates, without imposing prior information on the distribution of the underlying estimated parameters. This is pertinent in the mechanical engineering context, where the delta method was used previously for the uncertainty quantification of (A, C) and the resultant modal parameters in e.g. [10, 25–28], and for the uncertainty quantification of modal indicators in [47, 51]. Based on these established results, the delta method is applied to achieve a practical algorithm for the covariance computation related to estimates of (B, D).

First, the principles of the first-order delta method are recalled in the context of uncertainty propagation for subspace methods. A key element enabling the use of this statistical framework is the fact that the matrix $\mathcal{H}$ can be related to data covariance matrices $\widehat{\mathcal{R}}_j$, which are asymptotically Gaussian distributed [52]. For example, the matrix $\mathcal{H}_{\mathrm{dat}}$ in (9) for the N4SID method can be related to the data covariance matrices $\widehat{\mathcal{R}}_1, \ldots, \widehat{\mathcal{R}}_5$ as defined in (12) and (B.1) [10]. The sample covariances of these data covariance matrices can be easily obtained, and the idea is to propagate them onto $\mathcal{H}$ from the considered identification algorithm, and then to the estimates of (B, D) and $H(z)$.

Let $\widehat{\mathcal{R}}_1, \widehat{\mathcal{R}}_2, \ldots, \widehat{\mathcal{R}}_J$ be the data covariance matrices (computed on N data samples) that the chosen subspace algorithm depends on, including the matrices $\widehat{\mathcal{R}}_1, \widehat{\mathcal{R}}_2$ as defined in (12) that are in any case required for the estimation of B and D in Section 3.2. Let $\mathcal{R}_1, \mathcal{R}_2, \ldots, \mathcal{R}_J$ be their theoretical counterparts for $N \to \infty$, denote $\mathrm{vec}(\cdot)$ as the column-stacking vectorization operator and define the respective set of the vectorized data covariance matrices

$$\mathrm{vec}(\widehat{\mathcal{R}}) = \begin{bmatrix} \mathrm{vec}(\widehat{\mathcal{R}}_1) \\ \vdots \\ \mathrm{vec}(\widehat{\mathcal{R}}_J) \end{bmatrix}, \tag{18}$$

which is an estimate of the converged (unknown) vector $\mathrm{vec}(\mathcal{R})$ and satisfies the Central Limit Theorem (CLT) [10, 52]

$$\sqrt{N}(\mathrm{vec}(\widehat{\mathcal{R}}) - \mathrm{vec}(\mathcal{R})) \to \mathcal{N}(0, \Sigma_{\mathcal{R}}), \tag{19}$$

where $\Sigma_{\mathcal{R}}$ is the asymptotic covariance of $\mathrm{vec}(\widehat{\mathcal{R}})$. Now consider any matrix function of $\mathcal{R}$, $X = f(\mathcal{R})$, for which $\mathrm{vec}(X)$ is differentiable in $\mathrm{vec}(\mathcal{R})$ with a non-zero derivative $\mathcal{J}_{\mathcal{R}}^X \neq 0$. Assuming a consistent estimate $\widehat{X}$ of X, its first-order Taylor expansion yields

$$\mathrm{vec}(\widehat{X}) \approx \mathrm{vec}(X) + \mathcal{J}_{\mathcal{R}}^X(\mathrm{vec}(\widehat{\mathcal{R}}) - \mathrm{vec}(\mathcal{R})), \tag{20}$$

and from (19), the delta method states that an associated CLT holds for $\mathrm{vec}(X)$ as

$$\sqrt{N}(\mathrm{vec}(\widehat{X}) - \mathrm{vec}(X)) \to \mathcal{N}(0, \Sigma_X)$$

with the asymptotic covariance $\Sigma_X = \mathcal{J}_{\mathcal{R}}^X \Sigma_{\mathcal{R}} (\mathcal{J}_{\mathcal{R}}^X)^T$. This allows the propagation of the covariance related to $\widehat{\mathcal{R}}$ to any quantity $\widehat{X}$ that is computed from $\widehat{\mathcal{R}}$. Consistent estimates of the sensitivity $\mathcal{J}_{\mathcal{R}}^X$ and the covariance $\Sigma_{\mathcal{R}}$ are required for the estimation of Σ_X. The sensitivity $\mathcal{J}_{\mathcal{R}}^X$ can be obtained with the first-order perturbation $\mathrm{vec}(\Delta X) = \mathcal{J}_{\mathcal{R}}^X \mathrm{vec}(\Delta \mathcal{R})$, where $\Delta X = \widehat{X} - X$ and $\Delta \mathcal{R} = \widehat{\mathcal{R}} - \mathcal{R}$, neglecting the higher order terms. A consistent estimate of $\Sigma_{\mathcal{R}}$ can be easily obtained from a sample covariance, as detailed in [10]. In consequence, the covariance of $\mathrm{vec}(\widehat{X})$ is consistently approximated by $\frac{1}{N}\widehat{\Sigma}_X$.

With these tools, the first step in the covariance propagation can be carried out from $\widehat{\mathcal{R}}$ to $\mathcal{H}$ for the chosen subspace method, based on the relation

$$\mathrm{vec}(\Delta \mathcal{H}) = \mathcal{J}_{\mathcal{R}}^{\mathcal{H}} \mathrm{vec}(\Delta \mathcal{R}), \tag{21}$$

where $\Delta \mathcal{H}$ denotes the perturbation on the theoretical matrix $\mathrm{E}(\mathcal{H})$ when it exists. This has been done in detail in [10] and is outlined in Appendix B for the subspace methods related to $\mathcal{H}_{\mathrm{cov}}$ and $\mathcal{H}_{\mathrm{dat}}$. While the algorithm to estimate B and D in Section 3.2 is applicable for any subspace method, it requires estimates of the matrices Γ and U_{ker}, which are method-dependent as they are obtained from $\mathcal{H}$ in (11). Therefore, the uncertainties related to (B, D) will also depend on the uncertainties related to $\mathcal{H}$, as developed in the following section.

9

4.1. Covariance computation related to (B, D)

To derive the uncertainty related to (B, D), the first-order perturbation of (17) is developed as

$$\text{vec}\left(\Delta \begin{bmatrix} D \\ B \end{bmatrix}\right) = \text{vec}\left(\Delta \left(L_s^\dagger \mathcal{M}^v\right)\right) = \left(I_u \otimes L_s^\dagger\right) \text{vec}\left(\Delta \mathcal{M}^v\right) + (\mathcal{M}^{vT} \otimes I_{r+n})\text{vec}(\Delta L_s^\dagger), \tag{22}$$

where $\otimes$ denotes the Kronecker product. Matrices $\mathcal{M}^v$ and $L_s = LO_s$, as defined by (16), are computed from the data covariance matrices $\mathcal{R}_1$ and $\mathcal{R}_2$, as well as from the observability matrix Γ and its left null space U_{ker}, which both depend on $\mathcal{H}$ and thus on $\mathcal{R}$, related to the chosen subspace method. Hence, the uncertainty related to $\mathcal{M}^v$ and L_s in (22) can be fully linked to the uncertainty related to the collection of data covariance matrices in $\mathcal{R}$. The corresponding sensitivities are derived in detail in Appendix C, where the first-order perturbations related to $\mathcal{M}^v$ and $L_s^\dagger$ are developed with respect to $\mathcal{R}$ in Equations (C.4) and (C.13), respectively. Then they lead with (22) to the relation

$$\text{vec}\left(\Delta \begin{bmatrix} D \\ B \end{bmatrix}\right) = \mathcal{J}_\mathcal{R}^{D,B}\text{vec}\left(\Delta \mathcal{R}\right), \tag{23}$$

where the sensitivity $\mathcal{J}_\mathcal{R}^{D,B}$ is detailed in (C.15). The expression for the covariance of (B, D) follows as

$$\Sigma_{D,B} = \mathcal{J}_\mathcal{R}^{D,B}\Sigma_\mathcal{R}(\mathcal{J}_\mathcal{R}^{D,B})^T. \tag{24}$$

4.2. Covariance computation related to $H(z)$

The scheme to compute the covariance related to the estimates of $H(z)$ based on the covariance related to the estimates of (A, B, C, D) was proposed in [30, Sec. VII-B] and is recalled here for the sake of completeness. The method is general for any consistent input/output identification algorithm that provides the covariance $\Sigma_{A,B,C,D}$ related to the full set of state-space matrices (A, B, C, D). Together with the results of the previous section, this covariance is outlined in Appendix D for the considered subspace algorithms, and propagated to $H(z)$ as follows. Denote the real and imaginary part of a complex variable as $(\cdot)^{\text{R}}$ and $(\cdot)^{\text{I}}$, then $H^{\text{R}}(z) = CZ^{\text{R}}B + D$ and $H^{\text{I}}(z) = CZ^{\text{I}}B$ where $Z = (zI_n - A)^{-1}$. Then, their perturbations are linked to the state-space matrices by

$$\begin{bmatrix} \text{vec}(\Delta H^{\text{R}}(z)) \\ \text{vec}(\Delta H^{\text{I}}(z)) \end{bmatrix} = \underbrace{\begin{bmatrix} ((ZB)^T \otimes CZ)^{\text{R}} & I_u \otimes (CZ^{\text{R}}) & (Z^{\text{R}}B)^T \otimes I_r & I_{ru} \\ ((ZB)^T \otimes CZ)^{\text{I}} & I_u \otimes (CZ^{\text{I}}) & (Z^{\text{I}}B)^T \otimes I_r & 0_{ru,ru} \end{bmatrix}}_{=\mathcal{J}_{A,B,C,D}^{H(z)}} \begin{bmatrix} \text{vec}(\Delta A) \\ \text{vec}(\Delta B) \\ \text{vec}(\Delta C) \\ \text{vec}(\Delta D) \end{bmatrix}, \tag{25}$$

and the covariance of the corresponding stacked transfer matrix components follows as

$$\Sigma_{H(z)} = \mathcal{J}_{A,B,C,D}^{H(z)}\Sigma_{A,B,C,D}(\mathcal{J}_{A,B,C,D}^{H(z)})^T. \tag{26}$$

10

The transfer function is usually interpreted by the magnitude and phase of its components $H_{i,j}(z)$ corresponding to input j and output i, where $i = 1, \ldots, r$ and $j = 1, \ldots, u$. The magnitude and phase are given by $m_{i,j}(z) = |H_{i,j}(z)|$ and $p_{i,j}(z) = \tan^{-1}(H_{i,j}^{\mathrm{I}}(z)/H_{i,j}^{\mathrm{R}}(z))$, respectively, and their sensitivities yield

$$\begin{bmatrix} \Delta m_{i,j}(z) \\ \Delta p_{i,j}(z) \end{bmatrix} = \underbrace{\begin{bmatrix} |H_{i,j}(z)|^{-1} & 0 \\ 0 & |H_{i,j}(z)|^{-2} \end{bmatrix} \begin{bmatrix} H_{i,j}^{\mathrm{R}}(z) & H_{i,j}^{\mathrm{I}}(z) \\ -H_{i,j}^{\mathrm{I}}(z) & H_{i,j}^{\mathrm{R}}(z) \end{bmatrix}}_{=\mathcal{J}_{H_{i,j}(z)}^{m,p}} \begin{bmatrix} \Delta H_{i,j}^{\mathrm{R}}(z) \\ \Delta H_{i,j}^{\mathrm{I}}(z) \end{bmatrix}, \tag{27}$$

where $\Delta H_{i,j}^{\mathrm{R}}(z)$ and $\Delta H_{i,j}^{\mathrm{I}}(z)$ are found in the respective rows in (25). Denote their covariance by $\Sigma_{H_{i,j}(z)}$, which can be extracted from the corresponding rows and columns of $\Sigma_{H(z)}$ in (26). Then, the covariance of the magnitude and phase related to the output/input pair (i,j) follows as

$$\Sigma_{m,p}^{(i,j)} = \mathcal{J}_{H_{i,j}(z)}^{m,p} \Sigma_{H_{i,j}(z)} (\mathcal{J}_{H_{i,j}(z)}^{m,p})^T. \tag{28}$$

4.3. Algorithmic summary

The covariance computation related to (B, D) from Section 4.1 is outlined in Algorithm 1. The covariance computation related to the magnitude $m_{i,j}(z)$ and phase $p_{i,j}(z)$ of the transfer matrix component $H_{i,j}(z)$ from Section 4.2 is summarized in Algorithm 2.

Algorithm 1: Covariance related to (B, D).

Input : $\mathcal{H}$, $\widehat{\mathcal{J}}_{\mathcal{R}}^{\mathcal{H}}$ and $\widehat{\Sigma}_{\mathcal{R}}$ corresponding to the chosen subspace method as detailed e.g. in [10] ;

Output: Covariance $\widehat{\Sigma}_{D,B}$;

1 compute $\widehat{U}_{\mathrm{ker}}$ and $\widehat{\Gamma}$ in (11), and subsequently $\widehat{\mathcal{M}}^v$ and $\widehat{L}_s = \widehat{L}\widehat{O}_s$ based on (16) ;

2 compute sensitivity of $\mathcal{M}^v$ w.r.t. $\mathcal{R}$ in (C.4)–(C.6) using (C.1), (C.3) and (11) ;

3 compute sensitivity of $L_s^{\dagger}$ w.r.t. $\mathcal{R}$ in (C.13) using (C.3), (C.7)–(C.12) ;

4 compute $\widehat{\mathcal{J}}_{\mathcal{R}}^{D,B}$ with these sensitivities in (C.14)–(C.15) for the chosen subspace method ;

5 compute $\widehat{\Sigma}_{D,B}$ from $\widehat{\mathcal{J}}_{\mathcal{R}}^{D,B}$ and $\widehat{\Sigma}_{\mathcal{R}}$ in (24)

Algorithm 2: Covariance related to magnitude and phase of the transfer function.

Input : Estimates $(\widehat{A}, \widehat{B}, \widehat{C}, \widehat{D})$ and covariance $\widehat{\Sigma}_{A,B,C,D}$ for the chosen identification method (see Appendix D) ;

Output: Covariance $\widehat{\Sigma}_{m,p}^{(i,j)}$ for output/input pair (i,j) ;

1 compute $\widehat{\mathcal{J}}_{A,B,C,D}^{H(z)}$ in (25) and transfer matrix covariance $\widehat{\Sigma}_{H(z)}$ in (26) ;

2 compute $\widehat{\mathcal{J}}_{H_{i,j}(z)}^{m,p}$ in (27), and select $\widehat{\Sigma}_{H_{i,j}(z)}$ from $\widehat{\Sigma}_{H(z)}$ for the considered output/input pair (i,j) ;

3 compute covariance $\widehat{\Sigma}_{m,p}^{(i,j)}$ related to the magnitude and phase of $\widehat{H}_{i,j}(z)$ in (28)

---

5. Numerical validation

For the numerical validation of the proposed covariance computations consider a 6 DOF chain-like system as illustrated in Figure 1 that is modeled with spring stiffnesses $k_1 = k_3 = k_5 = 100$ N/m and

Table 1: Exact modal parameters of the chain system.

Natural frequency (Hz)						Damping ratio (%)					
f_1	f_2	f_3	f_4	f_5	f_6	ζ_1	ζ_2	ζ_3	ζ_4	ζ_5	ζ_6
1.936	5.618	8.682	14.494	15.798	17.007	2	2	2	2	2	2

$k_2 = k_4 = k_6 = 200$ N/m, mass $m_i = 1/20$ kg and a proportional damping matrix such that each mode has a damping ratio of 2%. The exact modal parameters of the system are depicted in Table 1.

The system is excited by a white noise signals in all DOFs and sampled with a frequency of 50 Hz. In addition, one known white noise input at DOF 1 is considered and the acceleration responses at DOFs 1, 4 and 6 are measured. Gaussian white noise with 5% of the standard deviation of the output is added to the response for each channel. The excitation is measured in N and the acceleration responses are in g.

The computations are performed in a Monte Carlo setup with $m = 1,000$ simulations of the described input and output signals. Three Monte Carlo experiments are performed that comprise the simulation of input and output data of different lengths, that is $N_1 = 10,000$, $N_2 = 100,000$ and $N_3 = 1,000,000$. Estimates of the system matrices (A, B, C, D) and the resultant transfer function $H(z)$ are evaluated using both the covariance-driven and the data-driven algorithms (see (9) and (10)), and the related covariance matrices are computed with the corresponding versions of Algorithm 1 and Algorithm 2.

5.1. Covariance related to (B, D)

Estimates of B are not unique since they are evaluated in an arbitrary state-space basis, thus not directly comparable with the exact B from the numerical model, nor suited for the computation of sample covariances for validation in the Monte Carlo experiments. Therefore, to validate estimates of B from (17) and their corresponding covariance from (24), we consider estimates of the product CB, which are independent of the state-space basis, and their covariance resulting from $\mathrm{vec}(\Delta(CB)) = (B^T \otimes I_r)\mathrm{vec}(\Delta C) + (I_u \otimes C)\mathrm{vec}(\Delta B)$. Since the uncertainty quantification for C has been validated in past works [10], the validity of the uncertainty quantification for B will follow. The uncertainty quantification for D can be performed directly, since this matrix does not depend on the state-space basis.
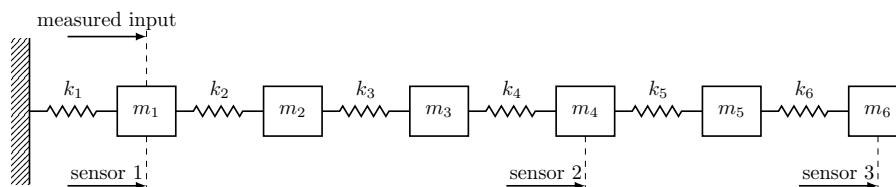

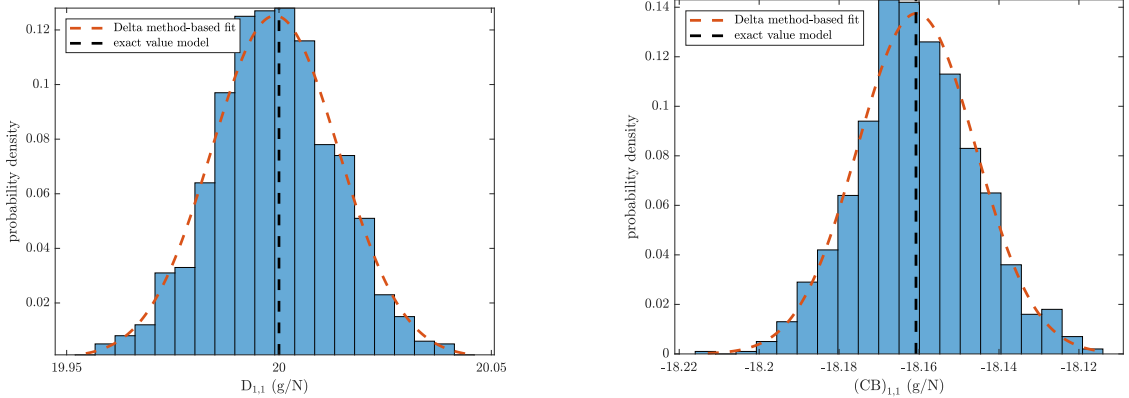Figure 1: Illustration of 6 DOF chain system used for Monte Carlo simulation.

Figure 2: Comparison of Monte Carlo estimates of $D_{1,1}$ and $(CB)_{1,1}$ to exact model value and delta method distribution fits for $N_2 = 100{,}000$, for covariance-driven subspace method.

First, D and CB and their respective covariance matrices are estimated with the covariance-driven algorithm. The comparison between the data-driven and the covariance-driven algorithms is presented later in this section. The estimates of D and CB from the Monte Carlo simulations yield histograms characterizing their underlying distribution function, which are shown in Figure 2 for the first components of D and CB, respectively. One can observe that the mean estimates of $D_{1,1}$ and $(CB)_{1,1}$ from the Monte Carlo simulations are close to their respective values from the model. Moreover, Gaussian fits obtained based on a covariance estimate using the delta method characterize the respective histograms well.

The validation of the covariance estimation with the proposed delta method-based computation is carried out as follows. The covariance is computed for each data set, from which the standard deviation is computed for the selected matrix entry $(1,1)$. These computed standard deviations should be directly comparable with the sample standard deviation of the Monte Carlo histogram computed from all the data sets. Consider estimates of $D_{1,1}$ and $(CB)_{1,1}$ for each Monte Carlo simulation $j = 1, \ldots, m$. Based on these values, it is straightforward to compute their sample means μ_{MC}^D and μ_{MC}^{CB}, as well as their sample standard deviations s_{MC}^D and s_{MC}^{CB} respectively, as a reference for comparison with the delta method-based standard deviations. Denote $\sigma_{\mathrm{DM},j}^D$ and $\sigma_{\mathrm{DM},j}^{CB}$ as the computed standard deviation of the estimates of $D_{1,1}$ and $(CB)_{1,1}$ in the j-th simulation. Their respective means denoted as $\bar{\sigma}_{\mathrm{DM}}^D$ and $\bar{\sigma}_{\mathrm{DM}}^{CB}$ should match the sample standard deviations s_{MC}^D and s_{MC}^{CB}, respectively. The sample standard deviation and the mean of the computed standard deviations with the developed method are shown together with their spread $(s_{\sigma_{\mathrm{DM}}^D}$ and $s_{\sigma_{\mathrm{DM}}^{CB}})$ in Table 2 for the covariance-driven and data-driven subspace methods. It can be seen that the compared standard deviations match very well, which suggests that the respective covariances are well-estimated with the proposed method. Moreover, the spread of the estimates is small. Note that the standard deviations of $(CB)_{1,1}$ estimated with the data-driven subspace method are consistently lower compared to those computed with the covariance-driven subspace method, as already stressed in [10]. The standard deviations are

13

Table 2: Comparison of standard deviations of $D_{1,1}$ and $(CB)_{1,1}$ from the proposed method ($\bar\sigma_{\mathrm{DM}}$) to the sample standard deviations (s_{MC}) for the covariance-driven and data-driven subspace methods. All units in are in (g/N).

Method	Data length	$s_{\mathrm{MC}}^{D} \times 10^{-2}$	$\bar\sigma_{\mathrm{DM}}^{D} \times 10^{-2}$	$s_{\sigma_{\mathrm{DM}}^{D}} \times 10^{-4}$	$s_{\mathrm{MC}}^{CB} \times 10^{-2}$	$\bar\sigma_{\mathrm{DM}}^{CB} \times 10^{-2}$	$s_{\sigma_{\mathrm{DM}}^{CB}} \times 10^{-4}$
	$N_1 = 10{,}000$	1.50	1.48	6.22	1.48	1.50	6.22
$\mathcal{H}_{\mathrm{cov}}$	$N_2 = 100{,}000$	0.67	0.67	2.63	0.68	0.68	2.71
	$N_3 = 1{,}000{,}000$	0.48	0.47	1.94	0.48	0.48	1.90
	$N_1 = 10{,}000$	1.49	1.48	6.23	1.42	1.45	6.06
$\mathcal{H}_{\mathrm{dat}}$	$N_2 = 100{,}000$	0.67	0.66	2.62	0.65	0.65	2.64
	$N_3 = 1{,}000{,}000$	0.47	0.47	1.93	0.46	0.46	1.83

Table 3: Percentage of Monte Carlo estimates in $\pm 2s_{\mathrm{MC}}$ intervals, and percentage of delta method-based intervals $\pm 2\sigma_{\mathrm{DM},j}$ containing the true value, each for $D_{1,1}$ and $(CB)_{1,1}$.

Method	Data length	s_{MC}^{D}–based CI	$\sigma_{\mathrm{DM},j}^{D}$–based CI	s_{MC}^{CB}–based CI	$\sigma_{\mathrm{DM},j}^{CB}$–based CI
	$N_1 = 10{,}000$	94.7%	94.5%	95.6%	95.9%
$\mathcal{H}_{\mathrm{cov}}$	$N_2 = 100{,}000$	96.5%	95.1%	95.3%	95.0%
	$N_3 = 1{,}000{,}000$	95.5%	95.2%	95.1%	95.4%
	$N_1 = 10{,}000$	94.5%	94.5%	95.1%	95.3%
$\mathcal{H}_{\mathrm{dat}}$	$N_2 = 100{,}000$	95.9%	94.9%	95.8%	94.7%
	$N_3 = 1{,}000{,}000$	95.3%	95.4%	95.3%	95.2%

decreasing with the data length, as expected.

The practical application of the proposed covariance computation is to obtain confidence intervals of the estimated parameters. Therefore to finalize this validation section, the merit of the computed confidence intervals is studied with the Monte Carlo experiments. Based on the histograms of the estimates of $D_{1,1}$ and $(CB)_{1,1}$, it is first verified that 95% of the Monte Carlo estimates are respectively in the $\pm 2s_{\mathrm{MC}}^{D}$ and $\pm 2s_{\mathrm{MC}}^{CB}$ interval around their true values from the model, for the chosen confidence level of $\gamma = 0.95$. The respective ratios are shown in the third and fifth columns of Table 3. Indeed, all values are very close to 95%, which indicates that the Gaussian distribution assumption is adequate for the confidence interval computation. Secondly, the quality of the delta-method based confidence intervals is examined, which are computed on each of the Monte Carlo estimates. According to the theory [53], 95% of them should contain the true value of the considered parameter. The respective ratios are shown in the fourth and last columns of Table 3. All values are again very close to 95%. This shows that the computed confidence intervals based on the Gaussian premise are accurate for all considered data lengths, which validates the proposed uncertainty quantification.

14

5.2. Covariance related to $H(z)$

First, the transfer function is evaluated for $0 < \omega_k \leq \omega_f$, $k = 1, \ldots, N_f$ where $N_f = 1024$ is the number of considered frequency lines, and its covariance is computed with the covariance-driven subspace method using Algorithm 2. Hereafter it will be illustrated that on average the delta-method based confidence intervals match the confidence intervals derived from the sample distribution of Monte Carlo histogram. For each discrete frequency, consider the delta-method based 95% confidence intervals of the phase $p_{1,1}$ and magnitude $m_{1,1}$ of the first transfer function component averaged over all the Monte Carlo estimates. These averaged intervals can be directly compared to the 95% confidence intervals derived from the sample distribution of the corresponding Monte Carlo estimates. For comparison, the respective intervals are centered around the true values of $p_{1,1}$ and $m_{1,1}$ from the model, which is illustrated in Figure 3. A comparison of the respective confidence intervals only is shown in Figure 4. Indeed, at each frequency the average delta-method based 95% confidence intervals match well with the 95% confidence intervals derived from the sample distribution of $p_{1,1}$ and $m_{1,1}$.
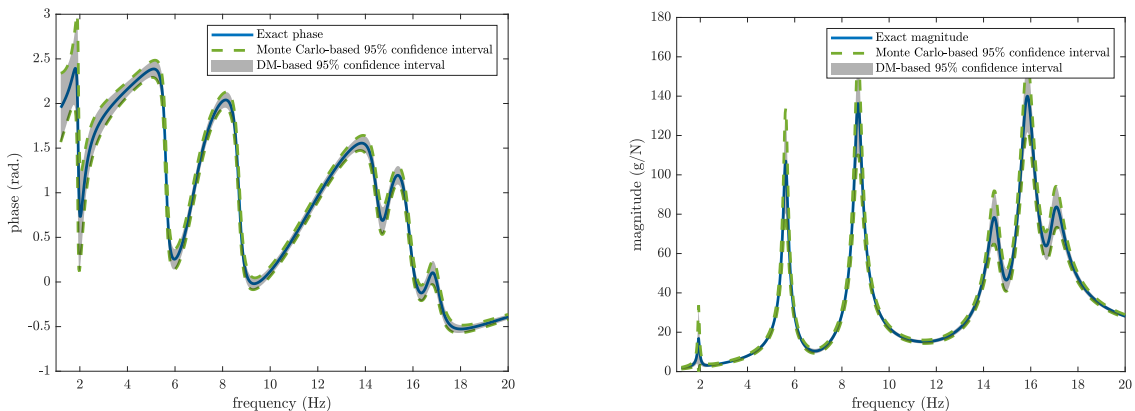

Figure 3: Exact first component of phase and magnitude of $H(z)$ with 20x zoomed Monte Carlo and delta method-based 95% confidence intervals for $N_2 = 100,000$.

Next, the merit of the Gaussian confidence intervals is studied with the Monte Carlo experiment. For each frequency line $k = 1, \ldots, N_f$ the sample standard deviation of the Monte Carlo histograms of $p_{1,1}(z)$ and $m_{1,1}(z)$ for $z = \mathrm{e}^{\mathrm{i}\omega_k T_s}$ are denoted respectively as $s^p_{\mathrm{MC},k}$ and $s^m_{\mathrm{MC},k}$. First, it is verified how many Monte Carlo estimates of the phase and magnitude at each frequency line k are in the $\pm 2s^p_{\mathrm{MC},k}$, $\pm 2s^m_{\mathrm{MC},k}$ interval around their true values from the model. The respective ratios, averaged over the investigated frequency lines, are shown in the third and fifth columns of Table 4. Secondly, the quality of the delta-method based confidence intervals is examined, which are computed for each of the $j = 1, \ldots, 1000$ Monte Carlo estimates at each frequency line k. The same procedure as in the previous section is applied, and it is verified how many Monte Carlo estimates are contained in the corresponding $\pm 2\sigma^p_{\mathrm{DM},j,k}$ and $\pm 2\sigma^m_{\mathrm{DM},j,k}$ intervals around
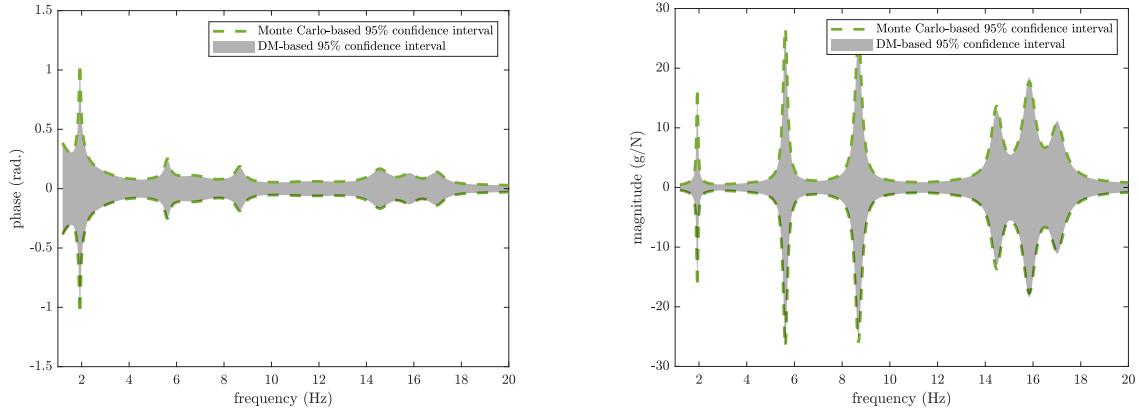
Figure 4: Zoomed x20 Monte Carlo and delta method-based 95% confidence intervals of the phase and the magnitude of $H(z)$ for $N_2 = 100,000$.

their true values. The respective ratios, averaged over the investigated frequency line, are shown in the fourth and last columns of Table 4. All values are again very close to 95%. This concludes the numerical validation section.

Table 4: Averaged ratio of Monte Carlo estimates in $\pm 2s^p_{\mathrm{MC,k}}, \pm 2s^m_{\mathrm{MC,k}}$ confidence interval, and averaged ratio of delta method-based $\pm 2\sigma^p_{\mathrm{DM},j,k}, \pm 2\sigma^m_{\mathrm{DM},j,k}$ confidence intervals containing the true value.

Method	Data length	s^p_{MC}–based CI	$\sigma^p_{\mathrm{DM},j}$–based CI	s^m_{MC}–based CI	$\sigma^m_{\mathrm{DM},j}$–based CI
	$N_1 = 10,000$	95.24%	94.97%	95.53%	95.28%
$\mathcal{H}_{\mathrm{cov}}$	$N_2 = 100,000$	95.61%	95.21%	95.36%	95.04%
	$N_3 = 1,000,000$	95.37%	94.89%	95.37%	95.15%
	$N_1 = 10,000$	95.36%	94.98%	95.46%	95.28%
$\mathcal{H}_{\mathrm{dat}}$	$N_2 = 100,000$	95.51%	95.07%	95.42%	95.01%
	$N_3 = 1,000,000$	95.26%	94.98%	95.39%	95.13%

6. Application

In this section, the proposed uncertainty quantification schemes are applied to assess the covariance of the transfer function in a laboratory experiment. For this purpose, a rectangular plate of high-density polyethylene plastic material of dimensions 53.5 x 32.0 x 2.3 cm and weight of 4.90 kg is used. The plate is designed so the first two elastic modes – torsion and bending, respectively – are close. The plate is supported by a layer of foam to ensure that the rigid body modes are sufficiently low in frequency for the purpose of this test.

The plate is subjected to uncorrelated continuous noise excitation from two small battery-operated
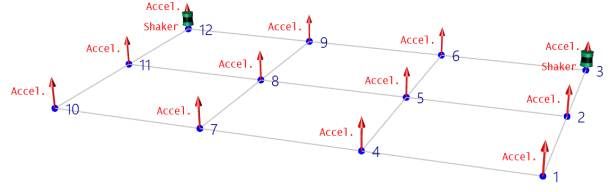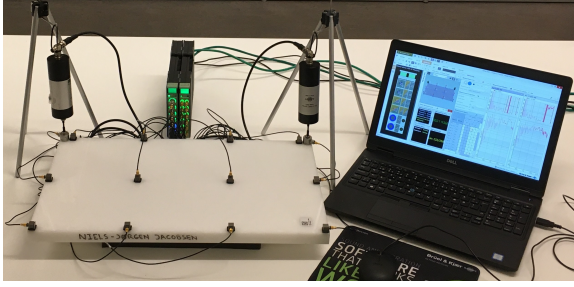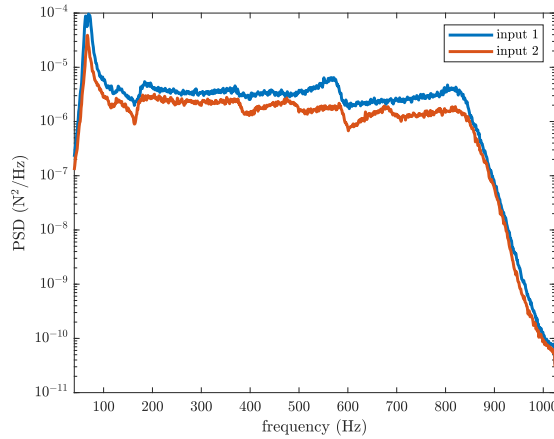
16

Figure 5: Experimental plate setup.

Figure 6: Power spectral density of the force inputs.

Hottinger Brüel & Kjær (HBK) type 5961 shakers. For simplicity, the shakers are hung above the plate knowing this arrangement creates some loading of the plate which is observable for the higher modes. The input force is measured with two HBK type 8230-001 force transducers and the response of the plate using 12 uniaxial HBK piezoelectric TEDS accelerometers with sensitivity of 100mV/g. Two hardware modules, HBK Type 3160-A-042 and Type 3053-B-120, are used for signal generation and input measurements, and a laptop computer for measurement control and analysis. The measurements are performed with a sampling frequency of 8192 Hz and a duration of 120 seconds. Prior to the uncertainty quantification of the transfer function, data are decimated to 2048 Hz. The experimental setup and the geometry of the plate are shown in Figure 5. The power spectral density (PSD) of the inputs is illustrated in Figure 6.

From Figure 6 it can be observed that the frequency response of the inputs is flat in the frequency band of the modes of interest. To estimate the modal parameters of the plate, both the covariance-driven and the data-driven input/output algorithms from Section 3.1 are applied, with $p = 7$ and the model orders ranging from $n_{\min} = 20$ to $n_{\max} = 50$. The covariance of the modal parameter estimates is computed with the corresponding algorithms detailed in [10]. In Figure 7 the resulting stabilization diagrams of natural frequencies with their respective 95% confidence intervals are shown. The natural frequency estimates are
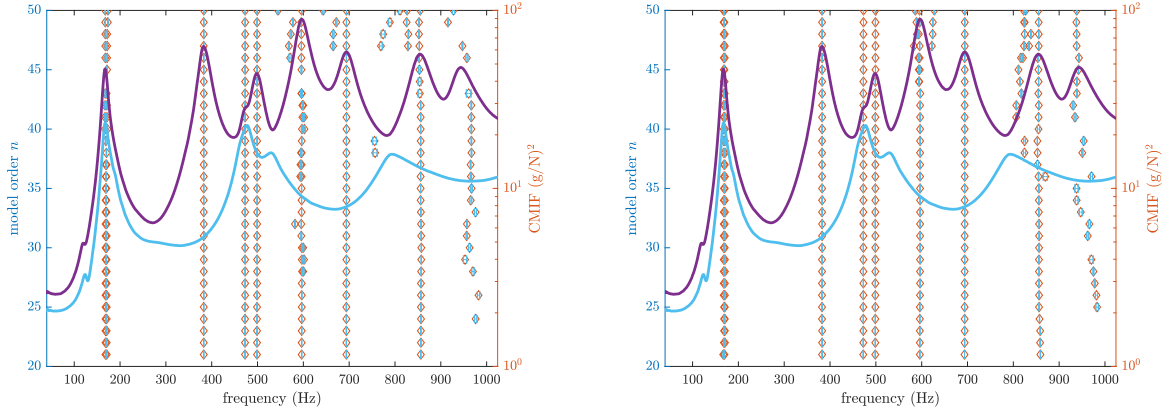
17

Figure 7: Stabilization diagram of natural frequencies with their 95% confidence intervals estimated with the covariance-driven (left) and data-driven (right) algorithms.

plotted together with the complex mode indicator function (CMIF) [54] evaluated from the estimates of the non-parametric FRFs. The peaks of the CMIF indicate the frequencies with dominant energy in the non-parametric FRF estimates and suggest a rough position of the natural frequencies of the structure [54]. By a visual inspection of the figure it can be viewed that the natural frequency estimates for every model order (red diamonds) stabilize on top of the peaks of CMIF and nine stable modes can be distinguished in the analyzed frequency range. Their natural frequencies and damping ratios estimated for $n_{\max} = 50$ are enclosed in Table 5 together with their standard deviations. It can be viewed that while the modal parameters estimates are *close* for both algorithms, their standard deviations are consistently higher for the covariance-driven approach. This can be also be conjectured when analyzing the uncertainty of the transfer function.

The transfer function is estimated from the quadruplet (A, B, C, D) using both the covariance-driven

Table 5: Modal parameters of the plate and their standard deviations estimated with the covariance-driven and the data-driven input/output subspace methods.

|	Method/Mode	1	2	3	4	5	6	7	8	9
$\mathcal{H}_{\mathrm{cov}}$	f [Hz]	167.70	173.61	382.79	472.99	499.07	596.26	694.05	855.03	927.64
	$\sigma_f \times 10^{-2}$ [Hz]	11.75	52.97	0.82	1.42	1.29	3.07	0.87	15.46	234.9
	ζ [%]	3.86	5.28	3.24	2.75	2.78	2.62	2.62	2.97	3.80
	$\sigma_\zeta \times 10^{-2}$ [%]	11.84	25.13	0.26	0.18	0.30	1.26	0.13	4.32	14.16
$\mathcal{H}_{\mathrm{dat}}$	f [Hz]	167.51	169.71	382.63	473.02	499.06	595.39	694.05	855.12	938.41
	$\sigma_f \times 10^{-2}$ [Hz]	5.03	8.29	0.46	0.42	0.64	7.13	0.52	9.13	63.17
	ζ [%]	4.18	5.53	3.21	2.71	2.82	2.42	2.61	2.99	3.03
	$\sigma_\zeta \times 10^{-2}$ [%]	6.13	5.97	0.13	0.14	0.14	1.71	1.00	1.30	7.75
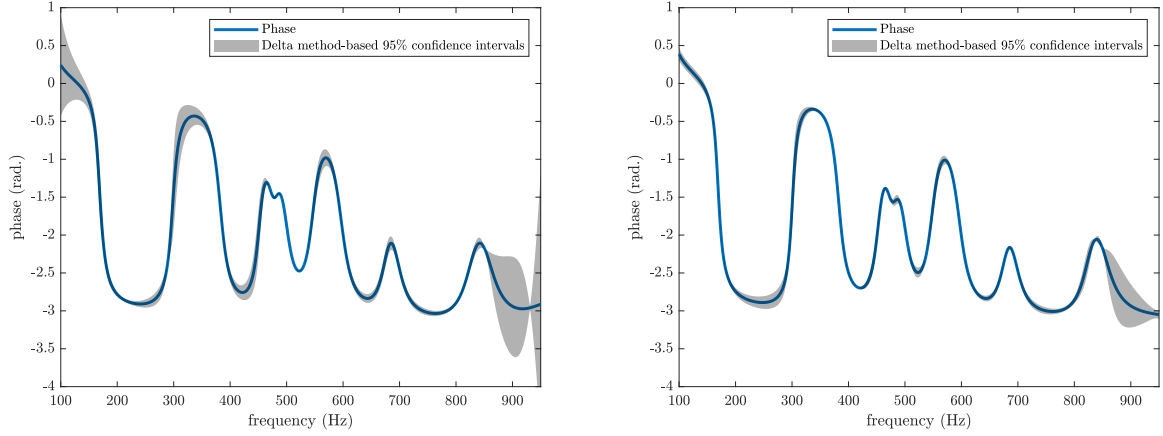
Figure 8: Phase of the first component of $H(z)$ with delta method-based 95% confidence intervals. The covariance-driven approach (left), the data-driven approach (right).
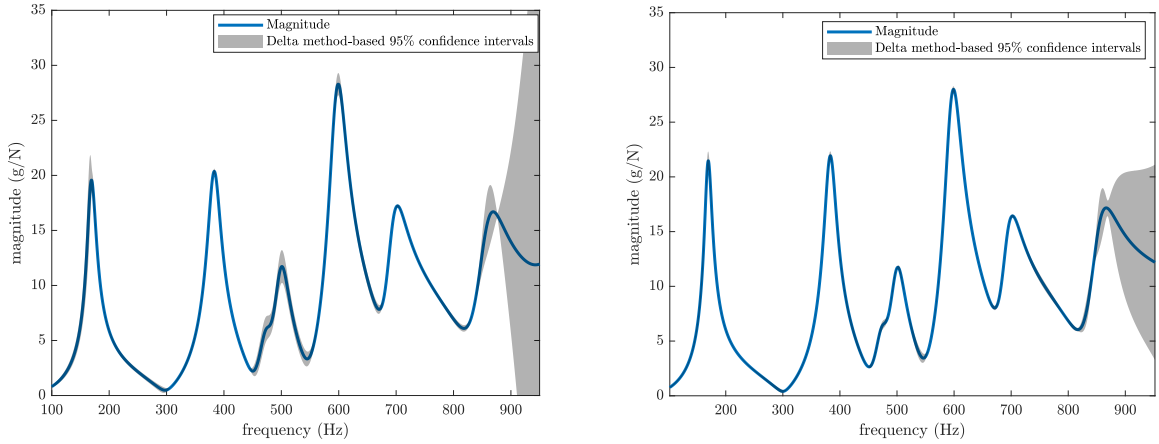

Figure 9: Magnitude of the first component of $H(z)$ with delta method-based 95% confidence intervals. The covariance-driven approach (left), the data-driven approach (right).

and the data-driven subspace methods at model order 20. The covariance of (B, D) estimates is evaluated for both subspace methods with Algorithm 1, and the covariance of the transfer function and its phase and magnitude are computed with Algorithm 2. The phase and the magnitude of the first component of the transfer function, with their 95% delta method-based confidence intervals are illustrated respectively in Figures 8 and 9. It can be seen that the frequency range for which the 95% confidence intervals of the phase and the magnitude are the largest corresponds well to the modal parameter estimates with the highest standard deviation depicted in Table 5. This is visible in particular for the second and the last modes of the plate, for which the estimates of the phase and the magnitude of the transfer function have a higher standard deviation when estimated with the covariance-driven approach.

To conclude this section, the confidence intervals computed with the delta method are compared to
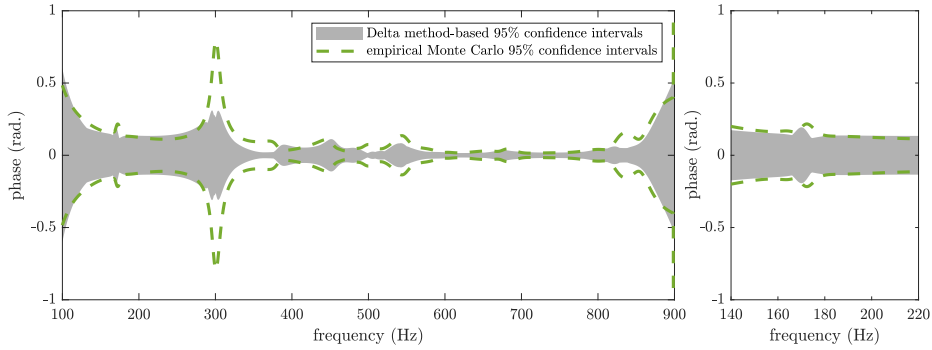
Figure 10: Empirical and delta method-based 95% confidence intervals of the phase of $H_{1,1}(z)$, using the data-driven subspace method.
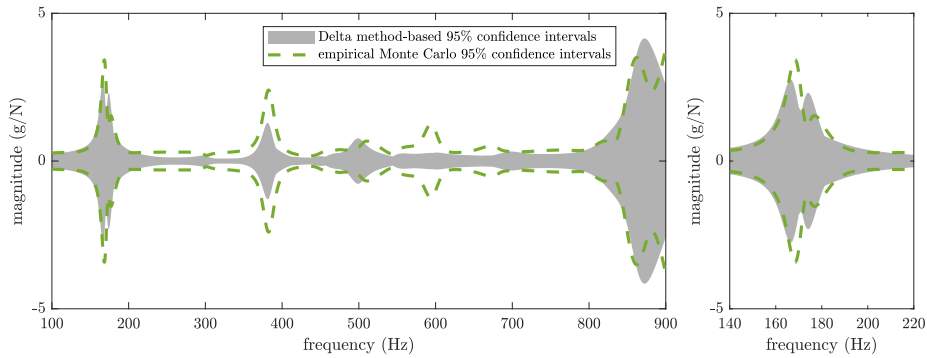

Figure 11: Empirical and delta method-based 95% confidence intervals of the magnitude of $H_{1,1}(z)$, using the data-driven subspace method.

confidence intervals computed empirically from the experimental data. For this, another data set was used that was separated into 32 data sets, each corresponding to 15 seconds of measurements. For each data set, the discrete transfer function is estimated from (A, B, C, D) with the data-driven subspace method using $p = 7$ and the model order $n = 20$ as before. Figures 10 and 11 respectively illustrate the confidence intervals computed empirically from the 32 estimates of the phase and magnitude of transfer function, and the computed delta method-based confidence intervals from one data set. The confidence intervals computed with the delta method match the empirical confidence intervals evaluated through Monte Carlo simulations. The precision of the latter is expected to improve if more data sets are used for the Monte Carlo simulations.

7. Conclusions

In this paper a direct expression has been developed for the covariance of estimates of the input-related matrices (B, D) in input/output subspace identification. Subsequently, this covariance, together with the covariance related to the estimates of (A, C), has been used to obtain the covariance of the transfer function

20

estimated from the state-space matrices. The proposed uncertainty quantification framework was validated on Monte Carlo simulations of a mechanical system, showing the accuracy of the derived expressions, and applied on data from a laboratory experiment for the identification of the transfer function and its uncertainties. Besides providing confidence bounds for system identification and the subsequent transfer matrix estimates, the proposed methodology can be used for uncertainty quantification in diverse applications, e.g. for transfer function-based damage detection, localization or model updating approaches. The covariance of the estimated quantities depends on the applied identification methods, where (A, C) can be estimated with several subspace methods, and different algorithms can be used to estimate (B, D). An optimal choice resulting in the smallest estimation covariance of the resulting transfer function will be analyzed in future work.

Appendix A. Proof of full column rank of L

To show that matrix $L \in \mathbb{R}^{p(pr-n) \times pr}$, defined as in (16), is of full column rank, its block rows can be permuted to

$$
L^{\text{perm}} = \begin{bmatrix}
\mathcal{L}_p & 0 & \dots & 0 & 0 \\
\mathcal{L}_{p-1} & \mathcal{L}_p & \dots & 0 & 0 \\
\dots & \dots & \dots & \dots & \dots \\
\mathcal{L}_2 & \mathcal{L}_3 & \dots & \mathcal{L}_p & 0 \\
\mathcal{L}_1 & \mathcal{L}_2 & \dots & \mathcal{L}_{p-1} & \mathcal{L}_p
\end{bmatrix}
$$

which is a lower triangular block matrix, and it is hence sufficient to show that $\mathcal{L}_p \in \mathbb{R}^{(pr-n) \times r}$ is of full column rank to obtain full column rank of L. For this, the left null space matrix $U_{\text{ker}} \in \mathbb{R}^{pr \times (pr-n)}$ of $\Gamma \in \mathbb{R}^{pr \times n}$ is constructed in the following, whose last block row is $\mathcal{L}_p^T$.

First, let the full QR decomposition of the observability matrix without the last block row

$$
\underline{\Gamma} = \begin{bmatrix} Q_1 & Q_2 \end{bmatrix} \begin{bmatrix} R \\ 0 \end{bmatrix}, \tag{A.1}
$$

be given, where $Q_1 \in \mathbb{R}^{(p-1)r \times n}$ and $Q_2 \in \mathbb{R}^{(p-1)r \times ((p-1)r-n)}$ are matrices with orthonormal columns and $Q_2^T Q_1 = 0$, and $R \in \mathbb{R}^{n \times n}$ is upper triangular. Since $\underline{\Gamma}$ is of full column rank with the condition $(p-1)r \geq n$ (see Section 2), the diagonal entries of R are non-zero. Note that Q_2 in the QR decomposition (A.1) only exists if $(p-1)r > n$, with the corresponding zero block below R on the right side.

Second, a full QR decomposition of Γ is constructed. Including the last block row of Γ in (A.1), it follows

$$
\begin{bmatrix} Q_1^T & 0 \\ Q_2^T & 0 \\ 0 & I_r \end{bmatrix} \Gamma = \begin{bmatrix} R \\ 0 \\ CA^{p-1} \end{bmatrix}. \tag{A.2}
$$

In order to cancel each entry of $CA^{p-1} \in \mathbb{R}^{r \times n}$ on the right side of (A.2), there exists a series of (orthogonal) Givens rotations $G_1, \ldots, G_{nr}$ such that [55]

$$G_{nr}^T \cdots G_2^T G_1^T \begin{bmatrix} Q_1^T & 0 \\ Q_2^T & 0 \\ 0 & I_r \end{bmatrix} \Gamma = G_{nr}^T \cdots G_2^T G_1^T \begin{bmatrix} R \\ 0 \\ CA^{p-1} \end{bmatrix} = \begin{bmatrix} \tilde{R} \\ 0 \\ 0 \end{bmatrix}, \tag{A.3}$$

where $\tilde{R} \in \mathbb{R}^{n \times n}$ is upper triangular. Hence, by solving (A.3), a full QR decomposition of Γ is given by

$$\Gamma = \underbrace{\begin{bmatrix} Q_1 & Q_2 & 0 \\ 0 & 0 & I_r \end{bmatrix} G_1 G_2 \cdots G_{nr}}_{=\tilde{Q}} \begin{bmatrix} \tilde{R} \\ 0 \\ 0 \end{bmatrix} = \tilde{Q} \begin{bmatrix} \tilde{R} \\ 0_{pr-n,n} \end{bmatrix}. \tag{A.4}$$

Now, the product of Givens rotations $G = G_1 G_2 \cdots G_{nr}$ is inspected more closely. Each of the rotations manipulates consecutively one of the first n rows as well as one of the last r rows in (A.3), but none of the rows in between (if they exist). Thus, the structure of G is

$$G = G_1 G_2 \cdots G_{nr} = \begin{bmatrix} G^{(11)} & 0 & G^{(13)} \\ 0 & I_{(p-1)r-n} & 0 \\ G^{(31)} & 0 & G^{(33)} \end{bmatrix}, \tag{A.5}$$

where $G^{(11)} \in \mathbb{R}^{n \times n}$, $G^{(33)} \in \mathbb{R}^{r \times r}$. Due to the structure of the consecutive Givens rotations, it can be easily checked that $G^{(33)}$ is an upper triangular matrix. Since the Givens rotations are based on the diagonal entries of R which are non-zero, it follows that the diagonal entries of $G^{(33)}$ are also non-zero, implying full rank.

Finally, the left null space U_{ker} is made explicit based on (A.4) and (A.5). It follows

$$\tilde{Q} = \begin{bmatrix} Q_1 G^{(11)} & Q_2 & Q_1 G^{(13)} \\ G^{(31)} & 0 & G^{(33)} \end{bmatrix},$$

where the first block column (containing n columns) corresponds to the image of Γ, and the remaining columns to its left null space. Hence U_{ker} is composed of the last two block columns of $\tilde{Q}$ and it follows $\mathcal{L}_p^T = \begin{bmatrix} 0 & G^{(33)} \end{bmatrix}$, which is of full row rank since $G^{(33)}$ has full rank. Thus, $\mathcal{L}_p$ has full column rank, as well as L.

While a particular left null space matrix U_{ker} was constructed in the proof, an arbitrary left null space of Γ is related to U_{ker} by the post multiplication of an invertible matrix, $U_{\text{ker}}T$. Hence, the property of full row rank of $\mathcal{L}_p^T T$ is valid for an arbitrary left null space basis. Note that the estimates of B and D are independent from the actual left null space basis, since a respective basis change T leads to a pre-multiplication by T^T of (14) and consequently by $(I_p \otimes T^T)$ of (16), which cancels out in (17).

22

Appendix B. Sensitivities related to $\mathcal{H}_{\mathrm{cov}}$ and $\mathcal{H}_{\mathrm{dat}}^s$

The derivation of the sensitivity $\mathcal{J}_{\mathcal{R}}^{\mathcal{H}}$ is straightforward for $\mathcal{H}_{\mathrm{cov}}$ since this matrix can be written directly in terms of data covariance matrices, but it is not direct for $\mathcal{H}_{\mathrm{dat}}$. Matrix $\mathcal{H}_{\mathrm{dat}}$ has no finite limit as $N \to \infty$ since its number of columns equals the number of samples N, hence its sample covariance estimate is undefined. However, the required estimates of Γ and U_{ker} for the identification of B and D (as well as A and C) would be equivalent if obtained from the "square" matrix $\mathcal{H}_{\mathrm{dat}}^s = \mathcal{H}_{\mathrm{dat}}\mathcal{H}_{\mathrm{dat}}^T$, thus their uncertainties can be derived from $\mathcal{H}_{\mathrm{dat}}^s$ that again is related directly to data covariance matrices [10]. Hence, the sensitivity $\mathcal{J}_{\mathcal{R}}^{\mathcal{H}}$ for the selected data-driven subspace method is evaluated for $\mathcal{H}_{\mathrm{dat}}^s$ in (21).

Besides the data covariance matrices $\widehat{\mathcal{R}}_1$ and $\widehat{\mathcal{R}}_2$ defined in (12), matrices $\mathcal{H}_{\mathrm{cov}}$ and $\mathcal{H}_{\mathrm{dat}}^s$ involve the data covariance matrices

$$\widehat{\mathcal{R}}_3 = \mathcal{Y}^+\mathcal{W}^{-T}, \ \widehat{\mathcal{R}}_4 = \mathcal{W}^-\mathcal{U}^{+T}, \ \widehat{\mathcal{R}}_5 = \mathcal{W}^-\mathcal{W}^{-T}, \widehat{\mathcal{R}}_6 = \mathcal{Y}^+\mathcal{Y}^{-T}, \ \widehat{\mathcal{R}}_7 = \mathcal{Y}^+\mathcal{U}^{-T}, \tag{B.1}$$

where $\mathcal{H}_{\mathrm{cov}} = f(\widehat{\mathcal{R}}_1, \widehat{\mathcal{R}}_2, \widehat{\mathcal{R}}_6, \widehat{\mathcal{R}}_7)$ and $\mathcal{H}_{\mathrm{dat}}^s = f(\widehat{\mathcal{R}}_1, \widehat{\mathcal{R}}_2, \widehat{\mathcal{R}}_3, \widehat{\mathcal{R}}_4, \widehat{\mathcal{R}}_5)$. Then, a first-order perturbation in the respective matrices $\mathcal{H}_{\mathrm{cov}}$ and $\mathcal{H}_{\mathrm{dat}}^s$ yields

$$\mathrm{vec}(\Delta\mathcal{H}_{\mathrm{cov}}) = \mathcal{J}_{\mathcal{R}}^{\mathcal{H}_{\mathrm{cov}}} \begin{bmatrix} \mathrm{vec}(\Delta\mathcal{R}_1) \\ \mathrm{vec}(\Delta\mathcal{R}_2) \\ \mathrm{vec}(\Delta\mathcal{R}_6) \\ \mathrm{vec}(\Delta\mathcal{R}_7) \end{bmatrix}, \quad \mathrm{vec}(\Delta\mathcal{H}_{\mathrm{dat}}^s) = \mathcal{J}_{\mathcal{R}}^{\mathcal{H}_{\mathrm{dat}}^s} \begin{bmatrix} \mathrm{vec}(\Delta\mathcal{R}_1) \\ \mathrm{vec}(\Delta\mathcal{R}_2) \\ \mathrm{vec}(\Delta\mathcal{R}_3) \\ \mathrm{vec}(\Delta\mathcal{R}_4) \\ \mathrm{vec}(\Delta\mathcal{R}_5) \end{bmatrix}, \tag{B.2}$$

where $\mathcal{J}_{\mathcal{R}}^{\mathcal{H}_{\mathrm{cov}}}$ and $\mathcal{J}_{\mathcal{R}}^{\mathcal{H}_{\mathrm{dat}}^s}$ are developed in [10].

Appendix C. Development of sensitivities related to (B, D)

First, the uncertainty related to $\mathrm{vec}(\mathcal{M}^v)$ is developed for (22), which is linked to $\mathrm{vec}(\mathcal{M})$ by (15)–(16) in a permutation, and subsequently to U_{ker}, $\mathcal{R}_1$ and $\mathcal{R}_2$ in its definition in (15). It holds $\mathrm{vec}(\Delta\mathcal{M}^v) = S_1\mathrm{vec}(\Delta\mathcal{M})$ with the permutation matrix

$$S_1 = \begin{bmatrix} I_p \otimes e_1^T \otimes I_{pr-n} \\ \vdots \\ I_p \otimes e_u^T \otimes I_{pr-n} \end{bmatrix} \tag{C.1}$$

where $e_j \in \mathbb{R}^u$ is a unit vector that is 1 at entry j. The first-order perturbation of $\mathcal{M}$ in (15) yields

$$\mathrm{vec}(\Delta\mathcal{M}) = \mathrm{vec}\left(\Delta(U_{\mathrm{ker}}^T\mathcal{R}_1\mathcal{R}_2^{-1})\right) = \left((\mathcal{R}_1\mathcal{R}_2^{-1})^T \otimes I_{pr-n}\right)\mathrm{vec}\left(\Delta U_{\mathrm{ker}}^T\right) + \left((\mathcal{R}_2^{-1})^T \otimes U_{\mathrm{ker}}^T\right)\mathrm{vec}(\Delta\mathcal{R}_1)$$
$$+ \left((\mathcal{R}_2^{-1})^T \otimes (-U_{\mathrm{ker}}^T\mathcal{R}_1\mathcal{R}_2^{-1})\right)\mathrm{vec}(\Delta\mathcal{R}_2), \quad \text{(C.2)}$$

using $\Delta(\mathcal{R}_2^{-1}) = -\mathcal{R}_2^{-1}\Delta(\mathcal{R}_2)\mathcal{R}_2^{-1}$. The left kernel sensitivity $\mathrm{vec}(\Delta U_{\mathrm{ker}}^T)$ was developed in [56] and writes

$$\mathrm{vec}(\Delta U_{\mathrm{ker}}^T) = \mathcal{J}_{\mathcal{H}}^{U_{\mathrm{ker}}^T}\mathrm{vec}(\Delta\mathcal{H}), \quad \mathcal{J}_{\mathcal{H}}^{U_{\mathrm{ker}}^T} = -(U_s D_s^{-1} V_s^T \otimes U_{\mathrm{ker}}^T). \tag{C.3}$$

Thus, combining (C.1)–(C.3) and (21) yields

$$\mathrm{vec}\left(\Delta\mathcal{M}^v\right) = \mathcal{J}_{\mathcal{R}}^{\mathcal{M}^{v,1}}\mathrm{vec}(\Delta\mathcal{R}) + \mathcal{J}_{\mathcal{R}_1}^{\mathcal{M}^{v,2}}\mathrm{vec}(\Delta\mathcal{R}_1) + \mathcal{J}_{\mathcal{R}_2}^{\mathcal{M}^{v,2}}\mathrm{vec}(\Delta\mathcal{R}_2), \tag{C.4}$$

$$\mathcal{J}_{\mathcal{R}}^{\mathcal{M}^{v,1}} = S_1\left((\mathcal{R}_1\mathcal{R}_2^{-1})^T \otimes I_{pr-n}\right)\mathcal{J}_{\mathcal{H}}^{U_{\mathrm{ker}}^T}\mathcal{J}_{\mathcal{R}}^{\mathcal{H}} \tag{C.5}$$

$$\mathcal{J}_{\mathcal{R}_1}^{\mathcal{M}^{v,2}} = S_1\left((\mathcal{R}_2^{-1})^T \otimes U_{\mathrm{ker}}^T\right), \quad \mathcal{J}_{\mathcal{R}_2}^{\mathcal{M}^{v,2}} = S_1\left((\mathcal{R}_2^{-1})^T \otimes -U_{\mathrm{ker}}^T\mathcal{R}_1\mathcal{R}_2^{-1}\right). \tag{C.6}$$

Second, the uncertainty related to $\mathrm{vec}(L_s^\dagger)$ is developed for (22), which is linked to L and O_s in (16) and thus to U_{ker} and Γ that are obtained from $\mathcal{H}$. The perturbation of $L_s^\dagger$ writes as [57]

$$\mathrm{vec}\left(\Delta L_s^\dagger\right) = \mathcal{J}_{L_s}^{L_s^\dagger}\mathrm{vec}(\Delta L_s), \ \mathcal{J}_{L_s}^{L_s^\dagger} = \left(L_s^{\dagger^T} \otimes -L_s^\dagger\right) + \left((I_{p(pr-n)} - L_s L_s^\dagger) \otimes (L_s^{\dagger^T} L_s^\dagger)^T\right)P_{p(pr-n),r+n}, \tag{C.7}$$

and $P_{a,b}$ is a permutation matrix such that for $X \in \mathbb{R}^{a,b}$ it holds $\mathrm{vec}(X^T) = P_{a,b}\mathrm{vec}(X)$ as defined in [27]. Next, the perturbation of $L_s = LO_s$ yields

$$\mathrm{vec}(\Delta L_s) = \left(O_s^T \otimes I_{pr}\right)\mathrm{vec}(\Delta L) + (I_{r+n} \otimes L)\mathrm{vec}(\Delta O_s). \tag{C.8}$$

The expression for L in (16) can be written as

$$L = \begin{bmatrix} \mathcal{L}_1 & \mathcal{L}_2 & \dots & \mathcal{L}_{p-1} & \mathcal{L}_p \\ \mathcal{L}_2 & \mathcal{L}_3 & \dots & \mathcal{L}_p & 0 \\ \mathcal{L}_3 & \mathcal{L}_4 & \dots & 0 & 0 \\ \dots & \dots & \dots & \dots & \dots \\ \mathcal{L}_p & 0 & \dots & 0 & 0 \end{bmatrix} = \begin{bmatrix} U_{\mathrm{ker}}^T S_{2,p} \\ U_{\mathrm{ker}}^T S_{2,p-1} \\ \vdots \\ U_{\mathrm{ker}}^T S_{2,1} \end{bmatrix}, \quad S_{2,k} = \begin{bmatrix} 0_{(p-k)r,kr} & 0_{(p-k)r,(p-k)r} \\ I_{kr} & 0_{kr,(p-k)r} \end{bmatrix}. \tag{C.9}$$

Thus, $L^T = \begin{bmatrix} S_{2,p}^T U_{\mathrm{ker}} & S_{2,p-1}^T U_{\mathrm{ker}} & \dots & S_{2,1}^T U_{\mathrm{ker}} \end{bmatrix}$ and the first-order perturbation of L yields

$$\mathrm{vec}(\Delta L) = P_{pr,p(pr-n)}\mathrm{vec}(\Delta L^T) = P_{pr,p(pr-n)}\underbrace{\begin{bmatrix} I_{pr-n} \otimes S_{2,p}^T \\ I_{pr-n} \otimes S_{2,p-1}^T \\ \vdots \\ I_{pr-n} \otimes S_{2,1}^T \end{bmatrix}}_{=S_3}\mathrm{vec}(\Delta U_{\mathrm{ker}}). \tag{C.10}$$

Next, based on (16) it holds

$$\mathrm{vec}(\Delta O_s) = S_4\mathrm{vec}(\Delta\Gamma), \quad S_4 = \begin{bmatrix} 0_{pr^2,(p-1)rn} \\ (I_n \otimes S_5) \end{bmatrix}, \quad S_5 = \begin{bmatrix} 0_{r,(p-1)r} \\ I_{(p-1)r} \end{bmatrix}\begin{bmatrix} I_{(p-1)r} & 0_{(p-1)r,r} \end{bmatrix}, \tag{C.11}$$

24

and the perturbation on Γ is linked to $\mathcal{H}$ through the SVD (11) by $\mathrm{vec}(\Delta\Gamma) = \mathcal{J}_{\mathcal{H}}^{\Gamma}\mathrm{vec}(\Delta\mathcal{H})$ as developed in detail in [26, 27]. It assumed that the non-zero singular values of $\mathcal{H}$ are distinct. Combining (C.8), (C.10) with (C.3) and (C.11) yields

$$\mathrm{vec}(\Delta L_s) = \mathcal{J}_{\mathcal{H}}^{L_s}\mathrm{vec}(\Delta\mathcal{H}), \quad \mathcal{J}_{\mathcal{H}}^{L_s} = (O_s^T \otimes I_{pr})S_3 \mathcal{J}_{\mathcal{H}}^{U_{\mathrm{ker}}^T} + (I_{r+n} \otimes L)S_4 \mathcal{J}_{\mathcal{H}}^{\Gamma}, \tag{C.12}$$

and the uncertainty on $(L_s)^{\dagger}$ is linked to $\mathcal{R}$ by combining (C.7), (C.12) and (21) as

$$\mathrm{vec}\left(\Delta L_s^{\dagger}\right) = \mathcal{J}_{\mathcal{R}}^{L_s^{\dagger}}\mathrm{vec}(\Delta\mathcal{R}), \quad \mathcal{J}_{\mathcal{R}}^{L_s^{\dagger}} = \mathcal{J}_{L_s}^{L_s^{\dagger}} \mathcal{J}_{\mathcal{H}}^{L_s} \mathcal{J}_{\mathcal{R}}^{\mathcal{H}}. \tag{C.13}$$

Finally, the sensitivity of (B, D) w.r.t. $\mathcal{R}$ as required in (23) is obtained by combining (22), (C.4) and (C.13), satisfying

$$\mathrm{vec}\left(\Delta\begin{bmatrix} D \\ B \end{bmatrix}\right) = \mathcal{J}_{\mathcal{R};1}^{D,B}\mathrm{vec}(\Delta\mathcal{R}) + \mathcal{J}_{\mathcal{R};2}^{D,B}\begin{bmatrix} \mathrm{vec}(\Delta\mathcal{R}_1) \\ \mathrm{vec}(\Delta\mathcal{R}_2) \end{bmatrix}, \tag{C.14}$$

where $\mathcal{J}_{\mathcal{R};1}^{D,B} = (I_u \otimes L_s^{\dagger})\mathcal{J}_{\mathcal{R}}^{\mathcal{M}^{v,1}} + (\mathcal{M}^{vT} \otimes I_{r+n})\mathcal{J}_{\mathcal{R}}^{L_s^{\dagger}}$, and $\mathcal{J}_{\mathcal{R};2}^{D,B} = (I_u \otimes L_s^{\dagger})\begin{bmatrix} \mathcal{J}_{\mathcal{R}_1}^{\mathcal{M}^{v,2}} & \mathcal{J}_{\mathcal{R}_2}^{\mathcal{M}^{v,2}} \end{bmatrix}$. Note that the sensitivity matrices $\mathcal{J}_{\mathcal{R}}^{\mathcal{M}^{v,1}}$ and $\mathcal{J}_{\mathcal{R}}^{(L_s)^{\dagger}}$ herein depend on the considered subspace method, and require plugging in the method-specific sensitivity matrix $\mathcal{J}_{\mathcal{R}}^{\mathcal{H}}$ as well as the respective data covariance matrices in $\mathcal{R}$ (see (18) and (B.2)). Since $\mathcal{R}_1$ and $\mathcal{R}_2$ are amongst the data covariance matrices considered in $\mathcal{R}$, both terms on the right hand side of (C.14) need to be combined to obtain the sensitivity $\mathcal{J}_{\mathcal{R}}^{D,B}$ in (23), in dependence of the considered subspace method. It follows

$$\mathcal{J}_{\mathcal{R}}^{D,B} = \mathcal{J}_{\mathcal{R};1}^{D,B} + \begin{bmatrix} \mathcal{J}_{\mathcal{R};2}^{D,B} & 0_{a,b} \end{bmatrix}, \tag{C.15}$$

where $a = (r+n)u$ and the number of columns b in the zero matrix depends on the size of the data covariance matrices that are required for the considered subspace method in addition to $\mathcal{R}_1$ and $\mathcal{R}_2$. For example, $b = p^2 r(r+u)$ in the considered covariance-driven method with $\mathcal{H}_{\mathrm{cov}}$ (see (B.2) left), and $b = 2p^2(r+u)^2$ in the considered data-driven method with $\mathcal{H}_{\mathrm{dat}}^s$ (see (B.2) right).

Appendix D. Covariance related to (A, B, C, D)

The sensitivities related to $H(z)$ are developed with respect to the state-space matrices (A, B, C, D) for the covariance propagation of these matrices to $H(z)$. So far, the covariance $\Sigma_{D,B}$ has been developed in this paper (see (23)–(24)), while the covariance propagation to $H(z)$ requires the covariance $\Sigma_{A,B,C,D}$ related to all state-space matrices defined in some basis. Selecting the appropriate rows of (23) yields

$$\mathrm{vec}(\Delta B) = \mathcal{J}_{\mathcal{R}}^{B}\mathrm{vec}(\Delta\mathcal{R}), \quad \mathrm{vec}(\Delta D) = \mathcal{J}_{\mathcal{R}}^{D}\mathrm{vec}(\Delta\mathcal{R}). \tag{D.1}$$

The sensitivities related to A and C with respect to $\mathcal{H}$ have been detailed in [26, 27] when computed as in Section 3.1, yielding

$$\text{vec}(\Delta A) = \mathcal{J}_{\mathcal{H}}^{A} \text{vec}(\Delta \mathcal{H}), \quad \text{vec}(\Delta C) = \mathcal{J}_{\mathcal{H}}^{C} \text{vec}(\Delta \mathcal{H}). \tag{D.2}$$

The developed sensitivities $\mathcal{J}_{\mathcal{H}}^{A}$ and $\mathcal{J}_{\mathcal{H}}^{C}$ from [26, 27] are not dependent on the chosen subspace method. Then, combining (D.1), (D.2), (19) and (21) yields

$$\sqrt{N} \begin{bmatrix} \text{vec}(\Delta A) \\ \text{vec}(\Delta B) \\ \text{vec}(\Delta C) \\ \text{vec}(\Delta D) \end{bmatrix} \to \mathcal{N}(0, \Sigma_{A,B,C,D}), \quad \text{where} \quad \Sigma_{A,B,C,D} = \begin{bmatrix} \mathcal{J}_{\mathcal{H}}^{A} \mathcal{J}_{\mathcal{R}}^{\mathcal{H}} \\ \mathcal{J}_{\mathcal{R}}^{B} \\ \mathcal{J}_{\mathcal{H}}^{C} \mathcal{J}_{\mathcal{R}}^{\mathcal{H}} \\ \mathcal{J}_{\mathcal{R}}^{D} \end{bmatrix} \Sigma_{\mathcal{R}} \begin{bmatrix} \mathcal{J}_{\mathcal{H}}^{A} \mathcal{J}_{\mathcal{R}}^{\mathcal{H}} \\ \mathcal{J}_{\mathcal{R}}^{B} \\ \mathcal{J}_{\mathcal{H}}^{C} \mathcal{J}_{\mathcal{R}}^{\mathcal{H}} \\ \mathcal{J}_{\mathcal{R}}^{D} \end{bmatrix}^{T} \tag{D.3}$$

With this result, the first-order perturbation in the real and imaginary parts of $H(z)$ are linked to the state-space matrices in (25).

References

[1] S. Greś, M. Döhler, L. Mevel, Variance computation for system matrices and transfer function from input/output subspace system identification, in: 21st IFAC World Congress, Berlin, Germany, 2020.

[2] P. van Overschee, B. de Moor, Subspace Identification for Linear Systems, 1st Edition, Springer, 1996.

[3] E. Reynders, G. De Roeck, Continuous vibration monitoring and progressive damage testing on the Z24 bridge, in: C. Boller, F. Chang, Y. Fujino (Eds.), Encyclopedia of Structural Health Monitoring, Wiley, 2009.

[4] D. Tcherniak, L. L. Mølgaard, Active vibration-based structural health monitoring system for wind turbine blade: Demonstration on an operating vestas V27 wind turbine, Structural Health Monitoring 16 (5) (2017) 536–550.

[5] D. Garcia, D. Tcherniak, An experimental study on the data-driven structural health monitoring of large wind turbine blades using a single accelerometer and actuator, Mechanical Systems and Signal Processing 127 (2019) 102 – 119.

[6] J. S. Nielsen, D. Tcherniak, M. D. Ulriksen, A case study on risk-based maintenance of wind turbine blades with structural health monitoring, Structure and Infrastructure Engineering 17 (3) (2021) 302–318.

[7] U. Füllekrug, M. Böswald, D. Göge, Y. Govers, Measurement of frfs and modal identification in case of correlated multi-point excitation, Shock and Vibration 15 (3, 4) (2008) 435–445.

[8] B. Peeters, W. Hendricx, J. Debille, H. Climent, Modern solutions for ground vibration testing of large aircraft, Sound & Vibration 43 (1) (2009) 8–15.

[9] E. Reynders, G. D. Roeck, Reference-based combined deterministic-stochastic subspace identification for experimental and operational modal analysis, Mechanical Systems and Signal Processing 22 (3) (2008) 617–637.

[10] P. Mellinger, M. Döhler, L. Mevel, Variance estimation of modal parameters from output-only and input/output subspace-based system identification, Journal of Sound and Vibration 379 (C) (2016) 1 – 27.

[11] L. Bull, P. Gardner, J. Gosliga, T. Rogers, N. Dervilis, E. Cross, E. Papatheou, A. Maguire, C. Campos, K. Worden, Foundations of population-based SHM, Part I: Homogeneous populations and forms, Mechanical Systems and Signal Processing 148 (2021) 107141.

[12] U. Lee, J. Shin, A frequency response function-based structural damage identification method, Computers & Structures 80 (2) (2002) 117 – 132.

[13] D. Bernal, Damage localization from the null space of changes in the transfer matrix, AIAA Journal 45 (2007) 374–381.

[14] X. Liu, N. Lieven, P. Escamilla-Ambrosio, Frequency response function shape-based methods for structural damage localisation, Mechanical Systems and Signal Processing 23 (4) (2009) 1243 – 1259.

[15] A. Esfandiari, F. Bakhtiari-Nejad, M. Sanayei, A. Rahai, Structural finite element model updating using transfer function data, Computers & Structures 88 (1) (2010) 54 – 64.

[16] M. Farshadi, A. Esfandiari, M. Vahedi, Structural model updating using incomplete transfer function and modal data, Structural Control and Health Monitoring 24 (7) (2017) e1932.

[17] E. Reynders, D. Degrauwe, G. D. Roeck, F. Magalhães, E. Caetano, Combined experimental-operational modal testing of footbridges, Journal of Engineering Mechanics 136 (6) (2010) 687–696.

[18] M. Deistler, K. Peternell, W. Scherrer, Consistency and relative efficiency of subspace methods, Automatica 31 (12) (1995) 1865 – 1875.

[19] D. Bauer, M. Deistler, W. Scherrer, Consistency and asymptotic normality of some subspace algorithms for systems without observed inputs, Automatica 35 (7) (1999) 1243 – 1254.

[20] A. Benveniste, L. Mevel, Nonstationary consistency of subspace methods, IEEE Transactions on Automatic Control 52 (6) (2007) 974–984.

[21] M. Verhaegen, Subspace model identification part 3. analysis of the ordinary output-error state-space model identification algorithm, International Journal of Control 58 (3) (1993) 555–586.

[22] M. Viberg, B. Wahlberg, B. Ottersten, Analysis of state space system identification methods based on instrumental variables and subspace fitting, Automatica 33 (9) (1997) 1603 – 1616.

[23] M. Jansson, Asymptotic variance analysis of subspace identification methods, IFAC Proceedings Volumes 33 (15) (2000) 91 – 96, 12th IFAC Symposium on System Identification, Santa Barbara, CA, USA.

[24] A. Chiuso, G. Picci, The asymptotic variance of subspace estimates, Journal of Econometrics 118 (1) (2004) 257 – 291.

[25] R. Pintelon, P. Guillaume, J. Schoukens, Uncertainty calculation in (operational) modal analysis, Mechanical Systems and Signal Processing 21 (6) (2007) 2359 – 2373.

[26] E. Reynders, R. Pintelon, G. De Roeck, Uncertainty bounds on modal parameters obtained from stochastic subspace identification, Mechanical Systems and Signal Processing 22 (4) (2008) 948 – 969.

[27] M. Döhler, L. Mevel, Efficient multi-order uncertainty computation for stochastic subspace identification, Mechanical Systems and Signal Processing 38 (2) (2013) 346–366.

[28] E. P. Reynders, Uncertainty quantification in data-driven stochastic subspace identification, Mechanical Systems and Signal Processing 151 (2021) 107338.

[29] E. Reynders, K. Maes, G. Lombaert, G. D. Roeck, Uncertainty quantification in operational modal analysis with stochastic subspace identification: Validation and applications, Mechanical Systems and Signal Processing 66-67 (2016) 13 – 30.

[30] E. Reynders, R. Pintelon, G. De Roeck, Consistent impulse-response estimation and system realization from noisy data, IEEE Transactions on Signal Processing 56 (7) (2008) 2696–2705.

[31] R. Pintelon, M. Hong, Asymptotic uncertainty of transfer-function estimates using nonparametric noise models, IEEE Transactions on Instrumentation and Measurement 56 (6) (2007) 2599–2605.

[32] R. Pintelon, J. Schoukens, Y. Rolain, Uncertainty of transfer function modeling using prior estimated noise models, IFAC Proceedings Volumes 36 (16) (2003) 1837 – 1842, 13th IFAC Symposium on System Identification (SYSID 2003), Rotterdam, The Netherlands.

[33] D. K. de Vries, P. M. van den Hof, Quantification of uncertainty in transfer function estimation: a mixed probabilistic-worst-case approach, Automatica 31 (4) (1995) 543 – 557.

[34] P. Verboven, P. Guillaume, B. Cauberghe, S. Vanlanduit, E. Parloo, A comparison of frequency-domain transfer function model estimator formulations for structural dynamics modelling, Journal of Sound and Vibration 279 (3) (2005) 775 – 798.

[35] P. Verboven, B. Cauberghe, P. Guillaume, Improved total least squares estimators for modal analysis, Computers & Structures 83 (25) (2005) 2077 – 2085.

[36] T. De Troyer, P. Guillaume, R. Pintelon, S. Vanlanduit, Fast calculation of confidence intervals on parameter estimates of least-squares frequency-domain estimators, Mechanical Systems and Signal Processing 23 (2) (2009) 261 – 273.

[37] T. De Troyer, P. Guillaume, G. Steenackers, Fast variance calculation of polyreference least-squares frequency-domain estimates, Mechanical Systems and Signal Processing 23 (5) (2009) 1423 – 1433.

[38] J. Schoukens, Y. Rolain, R. Pintelon, Analysis of windowing/leakage effects in frequency response function measurements, Automatica 42 (1) (2006) 27 – 38.

[39] R. Pintelon, J. Schoukens, G. Vandersteen, Frequency domain system identification using arbitrary signals, IEEE Transactions on Automatic Control 42 (12) (1997) 1717–1720.

[40] P. van Overschee, B. de Moor, N4SID: Subspace algorithms for the identification of combined deterministic-stochastic systems, Automatica 30 (1) (1994) 75 – 93.

[41] D. Bauer, M. Jansson, Analysis of the asymptotic properties of the MOESP type of subspace algorithms, Automatica 36 (4) (2000) 497 – 509.

[42] R. Bitmead, Persistence of excitation conditions and the convergence of adaptive schemes, IEEE Transactions on Information Theory 30 (2) (1984) 183–191.

[43] E. Gandino, L. Garibaldi, S. Marchesiello, Covariance-driven subspace identification: A complete input-output approach, Journal of Sound and Vibration 332 (26) (2013) 7000–7017.

[44] A. E. Ashari, L. Mevel, Input-output subspace-based fault detection, IFAC Proceedings Volumes 45 (20) (2012) 204 – 209, 8th IFAC Symposium on Fault Detection, Supervision and Safety of Technical Processes.

[45] L. Marin, M. Döhler, D. Bernal, L. Mevel, Robust statistical damage localization with stochastic load vectors, Structural Control and Health Monitoring 22 (3) (2015) 557–573.

[46] S. Greś, M. Döhler, P. Andersen, L. Mevel, Variance computation of the modal assurance criterion, in: Proceedings of the International Conference on Noise and Vibration Engineering (ISMA), Leuven, Belgium, 2018.

[47] S. Greś, M. Döhler, P. Andersen, L. Mevel, Uncertainty quantification for the modal phase collinearity of complex mode shapes, Mechanical Systems and Signal Processing 152 (2021) 107436.

[48] W. Favoreel, B. De Moor, P. Van Overschee, Subspace state space system identification for industrial processes, Journal of Process Control 10 (2) (2000) 149 – 155.

[49] E. Bura, R. Pfeiffer, On the distribution of the left singular vectors of a random matrix and its applications, Statistics & Probability Letters 78 (15) (2008) 2275–2280.

[50] G. Casella, R. L. Berger, Statistical Inference, 2nd Edition, Cengage Learning, 2001.

[51] S. Greś, M. Döhler, L. Mevel, Uncertainty quantification of the modal assurance criterion in operational modal analysis, Mechanical Systems and Signal Processing 152.

[52] E. J. Hannan, Multiple time series, Vol. 38, John Wiley & Sons, 1970.

[53] J. Neyman, H. Jeffreys, Outline of a theory of statistical estimation based on the classical theory of probability, Philosophical Transactions of the Royal Society of London. Series A, Mathematical and Physical Sciences 236 (767) (1937) 333–380.

[54] C. Shih, Y. Tsuei, R. Allemang, D. Brown, Complex mode indication function and its applications to spatial domain parameter estimation, Mechanical Systems and Signal Processing 2 (4) (1988) 367 – 377.

[55] G. H. Golub, C. F. Van Loan, Matrix Computations (3rd Ed.), Johns Hopkins University Press, Baltimore, MD, USA, 1996.

[56] E. Viefhues, M. Döhler, F. Hille, L. Mevel, Statistical subspace-based damage detection with estimated reference, Mechanical Systems and Signal Processing 164 (2022) 108241.

[57] G. H. Golub, V. Pereyra, The differentiation of pseudo-inverses and nonlinear least squares problems whose variables separate, SIAM Journal on Numerical Analysis 10 (2) (1973) 413–432.